Distribution characteristics of C-N-S microorganism genes in different hydraulic zones of high rank coal reservoirs in southern Qinshui Basin

Wei Shi[1], Shuheng Tang[2], Wenhui Huang[3], Songhang Zhang[3], and Zhongcheng Li[4]

[1]China University of Geosciences (Beijing)
[2]China University of Geosciences, Beijing
[3]China University of Geosciences (Beijing)
[4]China United Coalbed Methane Corporation Ltd.

November 24, 2022

Abstract

Microbial decomposition of carbon and biogenic methane in coal is one of the most important issues in CBM exploration. Microbial C-N-S functional genes in different hydraulic zones of high rank coal reservoirs was studied, demonstrating high sensitivity of this ecosystem to hydrodynamic conditions. The results shows that hydrodynamic strength of the 3# coal reservoir in Shizhuangnan block gradually weakened from east to west, forming the transition feature from runoff area to stagnant area. Compared with runoff area, the stagnant area has higher reservoir pressure, gas content and ion concentrations. The relative abundance of genes associated to C, N and S cycling was increased from the runoff area to stagnant area, including cellulose degrading genes, methane metabolism genes, N cycling genes and S cycling genes. This indicates that the stagnant zone had more active microbial C-N-S cycle. The machine learning model shows that these significantly different genes could be used as effective index to distinguish runoff area and stagnant area. Carbon and hydrogen isotopes indicate that methane in the study area was thermally generated. The methanogens compete with anaerobic heterotrophic bacteria to metabolize limited substrates, resulting in low abundance of methanogens. Meanwhile, the existence of methane oxidizing bacteria suggests biogenic methane was consumed by methanotrophic bacteria, which is the main reason why biogenic methane in the study area was not effectively preserved. In addition, weakened hydrodynamic conditions increased genes involved in nutrient cycling contributed to the increase of CO_2 and consumption of sulfate and nitrate from runoff area to stagnant area.

Posted on 24 Nov 2022 — CC-BY 4.0 — https://doi.org/10.1002/essoar.10506762.1 — This a preprint and has not been peer reviewed. Data may be preliminary.

Distribution characteristics of C-N-S microorganism genes in different hydraulic zones of high rank coal reservoirs in southern Qinshui Basin

Wei SHI [a,b,c], Shuheng TANG [a,b,c]11*Corresponding author, e-mail: tangsh@cugb.edu.cn , Wenhui HUANG[a,b,c], Songhang ZHANG [a,b,c], Zhongcheng LI [d]

a. MOE Key Lab of Marine Reservoir Evolution and Hydrocarbon Enrichment Mechanism, Beijing 100083, China

b. MOLR Key Lab of Shale Gas Resources Survey and Strategic Evaluation, Beijing 100083,China;

c. School of Energy Resources, China University of Geosciences (Beijing), Beijing 100083, China

d. China United Coalbed Methane Corporation Ltd., Beijing 100011, China

Abstract: Microbial decomposition of carbon and biogenic methane in coal is one of the most important issues in CBM exploration. Microbial C-N-S functional genes in different hydraulic zones of high rank coal

reservoirs was studied, demonstrating high sensitivity of this ecosystem to hydrodynamic conditions. The results shows that hydrodynamic strength of the 3# coal reservoir in Shizhuangnan block gradually weakened from east to west, forming the transition feature from runoff area to stagnant area. Compared with runoff area, the stagnant area has higher reservoir pressure, gas content and ion concentrations. The relative abundance of genes associated to C, N and S cycling was increased from the runoff area to stagnant area, including cellulose degrading genes, methane metabolism genes, N cycling genes and S cycling genes. This indicates that the stagnant zone had more active microbial C-N-S cycle. The machine learning model shows that these significantly different genes could be used as effective index to distinguish runoff area and stagnant area. Carbon and hydrogen isotopes indicate that methane in the study area was thermally generated. The methanogens compete with anaerobic heterotrophic bacteria to metabolize limited substrates, resulting in low abundance of methanogens. Meanwhile, the existence of methane oxidizing bacteria suggests biogenic methane was consumed by methanotrophic bacteria, which is the main reason why biogenic methane in the study area was not effectively preserved. In addition, weakened hydrodynamic conditions increased genes involved in nutrient cycling contributed to the increase of CO_2 and consumption of sulfate and nitrate from runoff area to stagnant area.

Keywords: coal bed methane; hydraulic zones; C-N-S microorganisms; genes; coal; water

1 Introduction

Understanding the mechanisms of biospheric characteristics in coal reservoir is important to CBM exploration (Tang et al., 2012; Wei et al., 2014; Guo et al., 2015; Wang et al., 2019). C-N-S microorganisms such as methanogens, nitrifying bacteria, denitrifying bacteria and sulfate reducing bacteria, play an important role in controlling the accumulation of coalbed methane, especially biogenic gas (Guo et al., 2012; Pashin et al., 2014; Schweitzer et al., 2019). Although such microorganisms regulate most biosphere processes related to fluxes of greenhouse gases like CO_2, CH_4 and N_2O, little is known about their role in coal reservoir. Through the systematically collection of water samples from coalbed methane wells in Southern Qinshui Basin for microbial sequencing and geochemical testing, it will show whether microorganisms' distribution changed in different hydrogeochemical zones of the coal seam.

Microorganisms mediate biogeochemical cycles of carbon (C), nitrogen (N), phosphorus (P), sulphur (S) in ecosystem dynamics. Fast developing metagenomic technologies allow us to explore the distribution characteristics and mechanism of microorganisms (Zhang et al., 2015; Wong et al., 2018). Integrated metagenomics technologies such as 16s RNA sequencing was used to determine the microbial community structure and functions structure in high rank coal ecosystem in Qinshui Basin.

Environmental factors such as redox conditions, pH, temperature and ion concentrations play an important role in controlling the distribution of various types of microorganisms, especially C-N-S microorganisms (Schlegel et al., 2011; Barnhart et al., 2013). These environmental factors are significantly changed in different hydraulic zones of Southern Qinshui Basin (Zhang et al., 2015). Therefore, this study predicts that hydrological conditions have important controlling effect on C-N-S microorganisms. The aim of this study is to find whether there is shifting microbial function composition from different hydrological zones, such as from runoff area to stagnant area. This study also tries to explain that if different microbial populations in different hydrological zones would have differential geochemical responses and that if weakened hydrodynamic conditions would greatly stimulate the functional genes involved in nutrient-cycling processes.

Southern Qinshui Basin located in north China craton is one of the most highly developed CBM region (Fig.1a) (Wang et al., 2016). Shizhuangnan block, in adjacent to Fanzhuang block and Zhengzhuang block (Fig.1b), is located in the transition area from the southeast edge of the basin to the deep part (Fig.2b). 3# coal seam is the main gas producing layer. The elevation of 3# coal is 223˜597m (Fig.2b), and the coal thickness is 4.45˜8.75m (Fig.2d). 3# coal seam in the study area has the highest coal rank (R^o_{max} 2.92˜3.02%) (Fig.2c) and the highest gas content (8˜25 m^3/t) in Qinshui Basin (Fig.2a). Now there are more than 1000 drainage wells in this block (Fig.1c). The daily average gas production of 570 drainage wells in Shizhuangnan block was counted and the gas production of most wells exceeded 1000 m^3/d. Moreover,

Posted on 24 Nov 2022 — CC-BY 4.0 — https://doi.org/10.1002/essoar.10506762.1 — This a preprint and has not been peer reviewed. Data may be preliminary.

high production wells were mainly distributed in the west of the block (Zhang et al., 2016).

Hydrogeological condition is an important controlling factor of coalbed methane enrichment (Xu et al., 2015; Yao et al., 2014). As the coal bearing strata in the study area are monoclinic structures extending from east to west, the synclines in the west weaken the hydrodynamic strength, the temperature and redox environment of the study area change dramatically from the oxidation runoff belt in the east of the basin edge to the deep stagnant area in the west (Zhang et al., 2015), making it an ideal area to research microbial distribution difference, the hydrogeological conditions of the study area will be introduced below.

2. Geological and hydrogeological conditions

The Qinshui Basin is a Carboniferous-Permian Basin. The outcrops of strata in Qinshui basin include the Cambrian, Ordovician, Permian, Triassic and Quaternary deposits (Fig.1d) (Zhang et al., 2015).

The coal-bearing strata are the Taiyuan and Shanxi Formations in the Upper Pennsylvanian and Lower Permian System (Fig.1e). The outcropping strata in and surrounding Shizhuangnan block include Ordovic Majiagou Group (O_2s), Fengfeng Group (O_2f); Carboniferous Benxi Group (C_2b), Taiyuan Group (C_3t); Permian Shanxi Group (P_1s), Shihezi Group (P_1x, P_2s) and Shiqianfeng Group (P_2sh); Triassic Liujiagou Group (T_1l), Heshanggou Group (T_1h), Ermaying Group (T_2er) and Tongchuan Group (T_2t) and some loose Quaternary layers including Pleistocene (Q_1, Q_2, Q_3) and Holoce (Q_4) (Fig.3a). The adjacent strata exhibit conformity contact, except the O_2f and C2b, which form a parallel unconformity contact. Shanxi Group consist fine-grained sandstones, coal, carbonates and shale, the average thickness is about 150 m (Fig.1e).

Shizhuangnan block is located in the northwest inclined slope belt of Qinshui Basin. The structure of the study area is striking NNE and dipping the west. The outcrop of the Jinhuo fault on the eastern edge of the basin has a relatively high elevation. Besides, the normal faults developed in the north of the block, including the Sitou Fault, the water blocking fault cuts the coal measure strata and controls the hydrodynamic field in the study area (Zhang et al., 2015).

There are five aquifers in Shizhuangnan block: the Ordovician aquifer, C3t aquifer, P1x-P1s aquifer, T1l-P2sh-P2s aquifer and Quaternary aquifer. The coal seam aquifers are confined by nearly impermeable mudstones or shales. So generally, the water production rates of 3# coal drainage wells are usually low. However, in the north of study area, faults connect coal reservoir with the roof aquifer, resulting in high water production rates in the north.

The elevation of the #3 coal seam gradually decreases from east to west (Fig.3b). The Jinhuo fault makes the Carboniferous-Permian strata exposed in the eastern part of the study area, where the atmospheric precipitation supplies and seeps from east to west along the monoclinic structure (Fig.3a). Because the Sitou fault in the west of the study area does not conduct water, with the coal seam and sandstone strata extending to the deep, the hydrodynamic conditions gradually weakened, forming the unique hydrogeological conditions of the transition from the east runoff area to the west stagnant area. The syncline in the western stagnant zones is the major high yield area of high production wells, with high salinity, high reservoir pressure and high gas content.

This study focused on the differences of C-N-S function genes between different hydrological zones and the relationship between microbial function structure and geochemical characteristics in the Southern Qinshui Basin. The stable isotopic compositions, major and minor ions in CBM co-produced water, were analyzed, the microbial species in the coal reservoir water at varying depths by 16S rRNA sequencing were investigated to evaluate microbial effects in the Shizhuangnan block.

3. Materials and Methods

3.1. Sample site and collection

A total of 23 CBM co-produced water samples were collected from the CBM wells in Shizhuangnan block in 2019.12, the sample distribution is shown in fig. 4a. All selected CBM wells have been running for more than 5 years constantly and the drainage coal seam is 3# coal. Water samples for ion and isotope analysis and

Posted on 24 Nov 2022 — CC-BY 4.0 — https://doi.org/10.1002/essoar.10506762.1 — This a preprint and has not been peer reviewed. Data may be preliminary.

16S rRNA sequencing were collected directly from the CBM wellhead in 500 mL headspace bottle and 50 mL centrifuge tubes. 0.5 L aluminum foil gas sampling bags were used for gas sampling. During collection, the whole container was filled with the water, placed on the ice, placed in the refrigerator, and immediately sent to the laboratory. All geochemical test including iron test and isotope test were completed in 7 days.

3.2 Ion concentration test

Ion chromatography instrument ICS-1100 (Thermo) was used for the determination of anions and cations. After the water sample was injected into the instrument, it was carried by the eluent and passed through the ion separation column. The conductivity detector was used to measure and record the peak heights of them in turn. From the standard curve drawn under the same conditions, the ion content in water sample could be calculated.

The chromatographic conditions of Cl^-、 NO_2^-、 NO_3^-、SO_4^{2-}were as follows: the column was AG19,4×250 mm; the eluent was KOH, 20 mm; the flow rate was 1 mL/min; the column temperature was 30 . The chromatographic conditions of Na^+、NH_4^+、K^+、Mg^{2+}、Ca^{2+}were as follows: the chromatographic column was CS12A,4×250 mm; the eluent was MSA, 20 mm; the flow rate was 1 mL/min; the column temperature was 30 .

3.3 Nitrogen and oxygen isotopes test

To determination nitrogen and oxygen isotope of nitrate. First, the pH value of the water sample was determined. The pH value of water samples was adjusted to be within the pH range of 6˜8 by hydrochloric acid (10%) and imidazole solution (2 mol/L). The nitrite was removed in advance with sulfonic acid solution, the amount of sulfonic acid added in the water sample was 1.5 times of that of nitrite, reacted at room temperature for at least 30 min, and then reacted in boiling water bath for 15 min to destroy the generated complex and eliminate the interference of nitrite.

After the two-step pre analysis, 40 mL of water sample was taken and put it into a 60 ml headspace bottle. 0.8mL of $CdCl_2$solution (20 g/L), 0.8ml of NH_4Cl solution (250 g/L) and 3x10 cm 4N (or 3N) clean zinc tablet (wiped clean with alcohol) were added and shaken on the shaker at a speed of 220 r/min for 20 min (full reaction). Then the zinc tablet was taken out, the empty bottle was closed to completed the nitrate reduction step. 2 mL of NaN_3 solution (2mol/L) and 1:1 mixture of CH_3COOH (20%) were added into the headspace bottle after nitrate reduction, and shaken violently to mix the sample and reagent. After shaking at 220 r/min for 30 min (full reaction), the azide reaction was ended by adding 1.2 mL NaOH solution (10 mol/L) as the termination agent (the solution was alkaline, which was not conducive to azide reaction).

Nitrate was converted into N_2O gas by the above chemical process reaction, and the nitrogen and oxygen isotope values of N_2O gas were measured by gas bench stable isotope mass spectrometer. The N_2O was carried into Mat 253 isotope ratio mass spectrometer to determine the nitrogen isotope ratio.

3.4 Water hydrogen and oxygen isotopes test

The hydrogen and oxygen isotopic composition of water was determined by Gasbench II-IRMS continuous flow. The constant temperature sample tray temperature was 28 , the poraplot Q chromatographic column temperature was 70 , and the He pressure was 120 kPa.

For δD-H_2O analysis, the water sample was packaged in a 2mL chromatographic bottle, covered with a hollow cap and placed on the sample rack. Hydrogen isotope in water was measured by high temperature pyrolysis method. The flow rate of carrier gas He was 100 mL/min, the temperature of reaction tube was 1380 , and the furnace temperature was 75 . Then the hydrogen isotope was measured by Delta V advantage isotope mass spectrometer. The calibration curves of hydrogen isotopes in water were established by inserting standard samples with different abundances before and after the samples.

For δ^{18}O-H_2O analysis, 200 μL water sample and standard water were taken and put into a 12 mL (labco) reaction bottle, and the cap was tightened. Then the air blowing needle was fixed, the working procedure of the automatic sampler was set, 0.3% of CO_2 + He mixture was filled in and inflated for 5 minutes to

Posted on 24 Nov 2022 — CC-BY 4.0 — https://doi.org/10.1002/essoar.10506762.1 — This a preprint and has not been peer reviewed. Data may be preliminary.

take the air from the bottle. After the completion of the filling, the water sample was kept in equilibrium for 18 hours, so that it could reach the equilibrium of isotope exchange. The CO_2 isotope ratio after the equilibrium of isotopic fractionation was determined by Delta V advantage isotope mass spectrometer with fixed injection needle.

3.5 DIC carbon isotope test

For one sample, 8 drops of anhydrous phosphoric acid was added to the 12 mL sample bottle (labco) and the bottle was put on the constant temperature sample disk in sequence. The air blowing needle was fixed, the working procedure of GC PAL automatic sampler was set, and the sample bottle was successively emptied with helium for 5min to remove the influence of the air in the bottle on the determination of C isotope ratio. 0.2mL water sample was added into the sample bottle, reacted at 45 °C on the dry heater for 45 minutes, and centrifugated before sample measurement.

The mixture of high purity helium and CO_2 was separated from other impurities by gas chromatography at 75 . The separated CO_2 is carried into Delta V detector by helium, and ionized by high-energy electron beam. After accelerated electric field, gaseous ions with different mass charge ratios (m/z44, m/z45, m/z46) enter the magnetic field to separate into different ion beams, which enter the receiver and convert them into electrical signals to determine the carbon isotope ratio. The accuracy of $\delta^{13}C_{DIC}$ value is ± 0.08

3.6 Methane isotope test

The instrument used in methane and carbon dioxide isotope analysis was the on-line analysis and test system (GC/C/IRMS) produced by ThermrFinnigan company, it mainly composed of Trace Ultra Chromatograph, combustion furnace (GC Combustion III) and stable isotope mass spectrometer Delta V Advantage. The mass spectrometry test conditions were set as follows: ion source high pressure was 3.0 kv, ion source emission current was 1.5 mA. The chromatography conditions were set as follows: Poraplot Q capillary column (27 mx0.32 mmx20.00 μm) was chosen as chromatographic column, high purity He (99.999%) was used as carrier gas, column flow rate was 1.5 mL/min, sample inlet temperature was 120 .

For δ^{13}C-CH_4 analysis, the temperature of the oxidation furnace (NiO/ CuO/ PI) was 960 and the temperature of the reduction furnace was 640 . Then methane was oxidized into carbon dioxide gas in combustion furnace, and then introduced into isotope mass spectrometer to detect carbon isotope value.

For δD-CH_4 analysis, the carrier gas was helium (1.2 mL/min), the split ratio was between 1:8 and 1:40 depending on methane concentration, and the temperatures of the GC oven and injector were 40°C and 200°C, respectively. Analysis of δD-CH_4involved on-line transfer of samples from a high temperature conversion reactor (containing an empty ceramic tube covered with graphite layer that was kept at a temperature of 1440°C) in which compounds were pyrolyzed to molecular hydrogen, carbon, and carbon monoxide, prior to their transfer into the mass spectrometer via a ConfloIV interface. Then molecular hydrogen was introduced into isotope mass spectrometer to detect hydrogen isotope value.

3.7 Gene extraction, PCR amplicon, and sequencing analysis

Water samples obtained from the CBM well for gene sequencing were stored in an incubator filled with dry ice under a low temperature condition (0) while being transferred to the laboratory. The DNA for each sample was extracted with FastDNA SPIN Kit (MP Biomedicals). DNAs were measured by PicoGreen dsDNA Assay Kit (Life Technologies) and subsequently diluted to 3.5 ng/μl. The V3-V4 region of the bacterial 16S rRNA gene was amplified by degenerate PCR primers 341F: CCTACGGGNGGCWGCAG and 805R: GACTACHVGGGTATCTAATCC. Each sample was amplified in triplicate (together with water control) in a 30 μl reaction system, which contained 3 μl of diluted DNA, 0.75 U PrimeSTAR HS DNA polymerase, 1 x PrimSTAR buffer (Takara), 0.2 mM deoxyribonucleoside triphosphates (dNTPs) and 10 pM of barcoded forward and reverse primers. After an initial denaturation step at 98 °C for 30 s, the targeted region was amplified by 25 cycles of 98 °C for 10 s, 55 °C for 15 s and 72 °C for 60 s, followed by a final elongation step of 5 min at 72 °C. If there was no visible amplification from negative control (no template added), triplicate PCR products were mixed and purified using an AMPure XP Kit (Beckman Coulter). The purified PCR

Posted on 24 Nov 2022 — CC-BY 4.0 — https://doi.org/10.1002/essoar.10506762.1 — This a preprint and has not been peer reviewed. Data may be preliminary.

products were measured by Nanodrop (NanoDrop 2000C, Thermo Scientific), and diluted to 10 ng/μl as templates for the second step of the PCR. All samples were amplified in triplicate with second-step primers, using identical conditions to the first step of the PCR but with eight cycles.

Technical replicates of each sample were combined and run on a 1.2% (w/v) agarose gel, and the bacterial 16S rRNA gene amplicons were extracted using a QIAquick Gel Extraction Kit (Qiagen). DNAs were subsequently measured with a PicoGreen dsDNA Assay Kit (Life Technologies) and 10 ng of each sample were mixed. Final amplicon libraries were purified twice using a Agencourt AMPure XP Kit (Beckman Coulter) and subjected to a single sequencing run on the HiSeq 2500 platform (Illumina Inc).

Bioinformatics analysis on 16S rRNA gene profiling. The 16S rRNA gene sequences were processed using QIIME v.1.9.1 and USEARCH v.10.0. The quality of the paired-end Illumina reads was checked by FastQC v.0.11.5 and processed in the following steps by USEARCH: joining of paired-end reads and relabeling of sequencing names; removal of barcodes and primers; filtering of low-quality reads; and finding non-redundancy reads.

Unique reads were clustered into OTUs with 97% similarity. OTUs were aligned to the SILVA database to remove sequences from chimera. The OTU table was generated by USEARCH. The taxonomy of the representative sequences was classified with the RDP classifier. Functional annotations of prokaryotic taxa were carried out using Picrust2 against the KEGG databases.

Three complementary non-parametric multivariate analyses, non-parametric multivariate analysis of variance (Adonis), analysis of similarity (ANOSIM), and the multi-response permutation procedure (MRPP;), were used to test the differences in soil microbial communities between warming and control treatments. The difference of the C-N-S function genes was detected by Welch's t-test with FDR correction in STAMP. The heatmaps were drawn by the "pheatmap" package.

A maximum likelihood phylogeny of main C-N-S microbes was generated from the aligned RDP sequence using Iqtree. All phylogenetic trees were edited in Itol.

To acquire the best discriminant performance of C-N-S microbes across runoff and stagnant area, we classified the abundances of bacterial taxa using the "randomForest" package. Cross-validation was performed by the rfcv function for selecting appropriate features. The varImpPlot function was used to show the importance of features in the classification.

4 Results and discussion

4.1 Geochemical results

Geochemical composition of CBM co-produced water is useful to identify hydraulic zone as water and rock interact along the flow paths. CBM co-produced water usually contained several important ions, with Na^+, K^+, Ca^{2+}, Fe^{3+}, Mg^{2+}, Cl^-, $HCO3^-$, $CO3^{2-}$, NO_3^- and $SO4^{2-}$accounting for most of the total solute in groundwater. Generally, shallow coal seam water in runoff area was characterized with lower KDS and higher Fe^{3+}, NO_3^- and $SO4^{2-}$contents, whereas deep coal seam water in stagnant area was characterized with higher KDS contents and lower Fe^{3+}, NO_3^- and $SO4^{2-}$contents.

The concentrations of Na^+ (K^+) in the water samples ranged from 241 to 1187 mg/L, whereas the concentrations of Cl^- ranged from 35 to 1609 mg/L. The concentrations of Ca^{2+} in the CBM co-produced water ranged from 0.12 to 10.7 mg/L. The concentrations of Mg^{2+} ranged from 0.57 to 4.31 mg/L. Dissolution of halite (NaCl) or sylvite (KCl) is the main source of Na^+ or K^+ in coal reservoir water. Additionally, silicates weathering could release Na^+or K^+, respectively. Cation exchange between Ca^{2+} or Mg^{2+} and Na^+ or K^+ can increase content of Na^+ and K^+ by reducing Ca^{2+} or Mg^{2+}. The water rock reaction in the stagnant area was more sufficient, which led to the increase of mineralization (KDS) in the stagnant area.

In contract, NO_3^-, $SO_4{}^{2-}$ and Fe^{3+} were more abundent in the runoff area, they are anaerobic electron acceptors closely realted to anaerobic respiration of microorganisms. The concentrations of NO_3^- ranged

Posted on 24 Nov 2022 — CC-BY 4.0 — https://doi.org/10.1002/essoar.10506762.1 — This a preprint and has not been peer reviewed. Data may be preliminary.

from 0.24 to 1.01 mg/L. The concentrations of SO_4^{2-} ranged from 6.93 to 17.02 mg/L. The concentrations of Fe^{3+} ranged from 0.3 to 5.57 mg/L.

The hydrogen and oxygen isotope composition of water could be used to identify the groundwater source. The following equation of atmospheric precipitation line in China was adopted: $\delta D = 7.9\delta^{18}O+8.2$. According to Fig. 7a, the water samples taken were distributed near the atmospheric precipitation line, indicating that the source of coal seam water is predominantly atmospheric precipitation.

The value of $\delta^{13}C_{CH4}$ ranged from -20 to -40and soluble methane samples suggested methane in the study area is thermogenic origin (Fig. 7b).

The value of $\delta^{15}N_{NO3}$ranged from -1 to -10suggesting the nitrate may come from biological nitrogen fixation or nitrification of NH_4^+ fertilizer on the ground (Fig. 7c).

4.2 Division of runoff area and stagnant area

The sampling was mainly in the south of Shizhuangnan block with the purpose of comparing the distribution differences of C-N-S functional genes between stagnant area and runoff area, so one of the most import issues in this study was to divide different hydrodynamic zones. Sever factors that change significantly were considered, as shown in the contour map.

The direct manifestation of hydrodynamic field is water pressure, so the three-dimensional hydrodynamic field in the sampling area was firstly modeled, and clearly the the water pressure rose sharply from east to the west on the edge of the western syncline (Fig. 5b), which was caused by the convergence of water flow in the low-lying area of the western stagnant area due to the Sitou fault which blocked water at the boundary.

The edge of the syncline in the west of the study area could be used as the boundary line to divide the hydrodynamic zones, as indicated by the black dotted line (Fig.4). Through this boundary, the atmospheric precipitation transit from the flowing state to the stagnant state, that was, from the runoff area to the stagnant area. The stagnant environment was conducive to the enrichment and preservation of coalbed methane. Indeed, the measured gas content had obvious changed across this line, from 7˜12 m^3/t to 14˜20 m^3/t (Fig.4). The stagnant environment made the interaction between water and rock stronger, resulting in higher mineralization in the stagnant area, which was also confirmed by the KDS concentration, as shown in the Fig. 6d. As there was transition from oxidation environment in runoff area to reduction environment in stagnant area, the geochemical data also support the above view, the concentration of NO_3^-, SO_4^{2-} , Fe^{3+} and $\delta^{13}C_{DIC}$, had obvious changed on both sides of this line, NO_3^-, SO_4^{2-} and Fe^{3+} were anaerobic electron acceptor in involved in several important anaerobic respiration processes, such as denitrification, sulfate reduction and iron reduction, their concentration were all reduced in the stagnant area's anoxic environment , shown in Fig. 6a˜6c.

It could be predicted that with the precipitation moving from east to west, the dissolved oxygen in water was gradually consumed, the aerobic respiration was weakened while the anaerobic respiration was enhanced, resulting in the consumption of anaerobic electron acceptors, such as NO_3^-, SO_4^{2-} and Fe^{3+} in the stagnant area. As the environment in the stagnant area was lack of oxygen supply, the anaerobic respiration was stronger than that in the runoff area, and the consumption of the electron acceptors was stronger in stagnant area.

Anaerobic respiration such as methanogenesis has isotope fractionation effect (Wang et al., 2016), resulting biogenic methane enriches lighter carbon and then aggravates dissolved inorganic carbon isotope (McCalley et al., 2014). If the methane production in stagnant area was stronger, the dissolved inorganic carbon isotope in stagnant area would be more positive than that in runoff area. The dissolved inorganic carbon isotope test results supported this view the C pool was isotopically fractionated by microbial methanogenesis or other microbial carbon cycling effect(Fig.6e).

Considering the structural location (Fig.6f), water pressure (Fig.5b), gas content (Fig.4) and geochemical data (Fig. 6a˜6e), the edge of syncline structure was selected as the boundary of dividing runoff area and

Posted on 24 Nov 2022 — CC-BY 4.0 — https://doi.org/10.1002/essoar.10506762.1 — This a preprint and has not been peer reviewed. Data may be preliminary.

stagnant area, as shown in Fig.5a, the red area was stagnant area, the blue area was runoff area, and the gray area in the north was fault developed deep coal.

In general, the structural location determined the hydrodynamic conditions, and then affected the distribution of hydrochemical field. This study pedicteded that the microbial functional genes involved anaerobic respiration such as denitrification, sulfate reduction were stronger in stagnant area. Next, this prediction would be proved by the gene sequencing results.

4.3 Microbial community functional structure

For the 23 water samples collected from CBM wells, 5 samples located in the runoff areas and 18 samples in the stagnant areas (Fig.5a). We generated a bacterial community profile for each sample via PCR amplification of the 16S ribosomal RNA (rRNA) gene targeting regions V3-V4 using primers 341F and 805R, followed by Illumina sequencing. 1966435 high-quality sequences from 23 samples were obtained (average, 85497; range, 53843-147971 reads per sample). High quality reads were analyzed with USEARCH, removing chimeric and organelle sequences, to produce 8264 operational taxonomic units (OTUs).

In all the samples, at the class level, Gammaproteobacteria, Betaproteobacteria, Deltaproteobacteria and Alphaproteobacteria were the most abundant bacteria, made up more than 85% of all microorganisms. Clostridia, Bacteroidia, Flavobacteriia, Bacilli, Methanobacteria, Actinobacteria were also present at higher relative abundance, but much lower than the four most abundant classes (Fig.8a).

90 most highly abundant microorganisms related to methanogenesis, denitrification, sulfate reduction and methane oxidation were selected. Maximum likelihood phylogenetic was constructed based on 16s V3-V4 sequences, shown in Fig.8b. There were three orders of Methanogens in study area, including Methanobacteriales, Methanomicrobiales and Methanosarcinales. Methane oxidizing bacteria included Methylococcales and Methylophilales. Denitrifying bacteria included Burkholderiales and Rhodobacterales. Sulfate reduction bacteria included Desulfobacterales and Desulfovibrionales. Aerobic ammonia oxidation bacteria (AOB) included Nitrosomonadales. Nitrification bacteria included Nitrospirales and Nitrosomonadales. The order of anammox bacteria was belonged to Candidatus Brocadiales.

Consistent with this expectation, the microbial community functional gene structure was different between runoff area and stagnant area. All of the nonparametric multivariate statistical tests of dissimilarity (MRPP, ANOSIM, and Adonis) showed that the overall functional structure of 3# coal production water's microbial communities was different between runoff area and stagnant area ($p < 0.005$, Table 1). Cluster analysis of C-N-S function genes showed that the samples from runoff area and stagnant area were completely clustered into two groups, which further indicated the functional differences of microorganisms between the two groups (Fig.11a).

The relative abundance of genes associated to C, N and S cycling was increased from the runoff area to stagnant area (Fig. 9). In contrast, only few functional genes, which mainly belong to functions related to assimilatory nitrate reduction, were significantly ($p < 0.005$) decreased in relative abundance in the stagnant area. Next, it will be discussed in detail.

4.3.1 C cycling

Changes in hydrodynamic conditions from runoff area to stagnant area significantly impacted a number of microbial functional groups important for C decomposition. 25 genes associated with decomposition of labile or recalcitrant C were detected. Among them, 9 genes exhibited higher relative abundance in stagnant area than runoff area samples ($p < 0.05$, Fig. 9a), including cellulose 1,4-beta-cellobiosidase (P = 2.64E-07), lichenase (P = 5.03E-06), alpha-mannosidase (P = 8.89E-05), 6-phospho-beta-glucosidase (P = 0.000490162), alpha-glucuronidase (P = 0.000582225), endo-1,4-beta-galactosidase (P = 0.000920978), endoglucanase (P = 0.002333825), chitinase (P = 0.002343304), beta-mannosidase (P = 0.018552947). Increases of the genes involved in recalcitrant C decomposition suggested the possible degradation of old recalcitrant C in stagnant area.

Posted on 24 Nov 2022 — CC-BY 4.0 — https://doi.org/10.1002/essoar.10506762.1 — This a preprint and has not been peer reviewed. Data may be preliminary.

This study held the idea that these recalcitrant C came from the plant debris on the ground. With the atmospheric precipitation moving from the eastern outcrop to the western stagnant environment in the study area, the temperature and pressure in the stagnant area were increased from the runoff area, which is more favorable for the degradation of recalcitrant C. The relative abundance of recalcitrant C decomposition genes was more than that of methanogenesis genes. In the case that the high rank coal in the study area was difficult to be degraded, the degradation of recalcitrant C from the surface would be an important substrate for microorganisms, and the monosaccharide produced could further provide substrates for other carbohydrate metabolism. As genes associated with mannose metabolism, carbohydrate hydrolases, lactose and galactose uptake and utilization, L-fructose utilization, xylose utilization and chitin utilization were all increased in the stagnant area (Supplementary Fig. 1). Overall, as these functional genes directly participate in C degradation, their higher abundance could enhance C decomposition and enhance methanogenesis and other anaerobic heterotrophic microorganisms such as nitrate reducing bacteria and sulfate reducing bacteria.

4.3.2 Methane metabolism

For all the methanogenesis genes resulted in Picrust2 analysis, the relative abundance of methanogenesis genes were increased from runoff area to stagnant area (Fig.9d), including mcrA, mcrB, mcrG, the key enzyme in all types of methanogenesis ($p < 0.00005$). FwdA-FwdH ($p < 0.00001$), mtd ($p < 0.00002$), mer ($p < 0.000002$), mtrA-mtrH ($p < 0.00002$), MvhADG–HdrABC ($p < 0.05$) in hydrogenotrophic methanogenesis showed more relative abundance in stagnant area too. Codh–Acs ($p < 0.00007$) in aceticlastic methanogenesis and MtaA-MtaC ($p < 0.00008$) in methylotrophic methanogenesis were also more abundant in stagnant area. What's more, fbiC ($p < 0.03$), cofH, cofG, cofC, cofD and cofE ($p <0.0006$) in F_{420} biosynthesis, mfnB, mfnD, mfnE, mfnF ($p < 0.02$) in methanofuran biosynthesis and comC, comE, comD ($p <0.00002$) in Coenzyme M biosynthesis were increased in the stagnant area. Suggesting an increase of all types of methanogenesis in the western stagnant area.

In both the runoff area and stagnant area samples there was a greater relative abundance of pmoB (a gene encoding particulate methane monooxygenase subunit B) than any methanogenesis genes, suggesting that of the biogenic methane could be oxidized aerobically (Treude et al., 2014). Indeed, the exploitation of CBM wells, including drilling and hydraulic fracturing, increased the opening degree and oxygen content of the coal seam, resulting in a high relative abundance of methane oxidizing bacteria in the samples. These aerobic bacteria grew in the wellbore or drainage outlet, consuming the dissolved methane of the produced water, which explained why there was methanogenesis microorganisms in the study area, but biogenic methane had not been effectively preserved. The aerobic and anaerobic oxidation of methane might have an important consumption mechanism of biogenic gas in the process of CBM generation history, although anaerobic methane oxidizing bacteria (ANME and M. oxyfera) were not detected in the 16S sequencing of our recently collected water samples.

Because the isotope characteristics of both the methane gas samples and the water-soluble methane samples showed complete thermogenic (Fig.7b), there were two possibilities that biogenic gas does not exist: (1) In most of the historical methane generation process, due to the unsuitable temperature and pressure conditions, methanogens did not exist or exist in the low abundance. The methanogens began to grow only when the outcrop of uplifted coal seams received meteoric water supply of organic matter and minerals. (2) In the gas generation stage of coalbed methane, the existence of methanogens was accompanied by aerobic and anaerobic oxidation methylotrophic bacteria, and biogenic methane was consumed by these microorganisms (Evans et al., 2019). In addition, because methanogens and sulfate reducing bacteria shared the same substrate H_2, this competition mechanism further compressed the living space of methanogens, resulting in that biogenic methane is not rich in the study area.

4.3.3 N cycling

Nitrogen, including nitrate, nitrite and ammonium, is an important element for all microorganisms and is required for the biosynthesis of key cellular components such as amino acid and nucleotide (Wenk et al., 2014; Kuypers et al., 2018; Tian et al., 2016; Shen et al., 2015; Hu et al., 2014). 25 genes associated with N

Posted on 24 Nov 2022 — CC-BY 4.0 — https://doi.org/10.1002/essoar.10506762.1 — This a preprint and has not been peer reviewed. Data may be preliminary.

cycling were detected, including nitrogen fixation, anaerobic oxidation of ammonia, nitrification, anammox, dissimilatory nitrate reduction, assimilatory nitrate reduction and denitrification. There were also different genes involved in N cycling between runoff area and stagnant area (Fig. 9b), Most (56%) of the Picrust2-detected functional genes involved in N cycling were increased from runoff area to stagnant area ($p < 0.05$; Fig. 9b), consistent with the previous prediction that weakened hydrodynamic conditions enhances nutrient cycling.

For example, the abundance of N_2-fixing genes was higher in response to hydrodynamic conditions ($p < 0.05$; Fig. 9b), the nifD ($p = 0.00007$), nifH ($p = 0.0001$), nifK ($p = 0.0007$) had higher abundance in the stagnant samples. In addition, weakened hydrodynamic strength from runoff area to stagnant area seemed to decrease dissimilatory nitrate reduction and increase nitrification, denitrification processes, as indicated by decreased narG ($p = 0.017$), narH ($p = 0.02$), narI ($p = 0.01$) gene, and increased nirK ($p = 0.008$), nosZ ($p = 0.00002$), norC ($p = 0.001$), napA ($p = 0.0008$), napB ($p = 0.0005$), nrfA ($p = 0.000004$), and amoB ($p = 0.04$) gene from runoff area to stagnant area (Fig. 9b). The increase in nitrification gene amoB and N_2-fixing gene nifDH would lead to higher nitrite and nitrate concentrations, which was also supported by the greater abundance of genes for various reductive processes which used nitrate as an electron acceptor, such as nirK, nosZ, norC for denitrification, nrfA for dissimilatory nitrate reduction to ammonium (narG, narH, narI, napA, napB shared by denitrification and dissimilatory nitrate reduction) and nirA for assimilatory nitrate reduction (Fig. 9b). Significant different N-cycle related genes between the two groups were labeled on the N pathway map, as shown in Fig.11b.

Almost all the N cycling genes were more abundant in the stagnant area, except dissimilatory nitrate reduction, were more abundant in the runoff area. This was possible, as NO_3^-concentration decreased from runoff area to stagnant area, suggesting the consumption of nitrate in runoff area by the first step of dissimilatory nitrate reduction. Reduction products such as nitrite would continue to converge into the stagnant area, and then be reduced by denitrification microorganisms, resulting in the increase of denitrification genes, such as nirK, norC and nosZ. The increased relative abundance of N cycling genes (N fixation and nitrification) and other nutrient-cycling genes could increase nutrient (especially N) availability in stagnant coal reservoirs, which is important for ecosystem C dynamics because N is a limiting factor for microorganism growth in most groundwater ecosystems. The enhanced N uptake could in turn affect C metabolism such as cellulose, mannose metabolism, carbohydrate metabolism, which increased in response to hydrodynamic conditions.

As the nitrogen and oxygen isotopes of nitrate shows that nitrate may come from surface soil and fertilizer (Fig. 7c), which seep into stagnant area with meteoric water, some nitrate may also come from the nitrogen fixation and of in-situ microorganisms in coal seam itself.

4.3.4 S cycling

Sulfur metabolism in microorganisms consists of redox reactions of organic and inorganic sulfur substrates that can play a major part in the biogeochemical cycle (Zerkle et al., 2010; Zopfi et al., 2008; Li et al., 2010; Treude et al., 2014; Gomes et al., 2017). As the same of denitrification, sulfate reduction is an anaerobic respiration that might be stronger in stagnant area. Nine of the fourteen detected sulfur metabolic genes had higher relative abundance in stagnant area than in runoff area (Fig.9c), suggesting enhanced microbial functional capacity for S cycling in stagnant area. These genes included dsrAB encoding dissimilatory sulfite reductase ($p < 0.001$), sir encoding sulfate reductase ($p = 0.003$), cysN encoding sulfate adenylyltransferase ($p = 0.008$), sat encoding sulfate adenylyltransferase ($p = 0.00008$), aprAB encoding adenylylsulfate reductase ($p < 0.02$) and PAPSS encoding 3'-phosphoadenosine 5'-phosphosulfate synthase ($p = 0.03$).

4.4 Machine-learning classification C-N-S genes between runoff area and stagnant area

As C-N-S genes changed significantly between runoff area and stagnant area, they could be used as biomarkers to differentiate water samples of runoff area and stagnant area. The prediction model was established using a random-forest machine-learning method to correlate runoff area and stagnant area with Picrut2 data (Subramanian et al., 2014; Yatsunenko et al., 2014; Karlsson et al., 2014). Ten-fold cross-validation with five repeats was carried out to evaluate the importance of indicator bacterial families. The cross-

Posted on 24 Nov 2022 — CC-BY 4.0 — https://doi.org/10.1002/essoar.10506762.1 — This a preprint and has not been peer reviewed. Data may be preliminary.

validation error curve stabilized when the most relevant genes were used (Fig.12b). These genes included methanogenesis genes (mtr, fwd, mcr, mtd, mtr, hdr, mer and mvh); aceticlastic methanogenesis gene (cdh); F_{420}biosynthesis gene (cof); Coenzyme M biosynthesis gene(com); dissimilatory and assimilatory sulfate reduction genes (sat, sir, dsr and apr); assimilatory nitrate reduction genes (napA and nrfA) and denitrification gene (nosz). Fig.12a showed the above-mentioned functional genes' relative abundence in runoff area samples and stagnant area samples. This consisted with the Welch's t-test results. As these function genes related to methanogenesis, nitrate reduction and sulfate reduction were all anaerobic respiration genes, when the hydrogeological environment transits from the aerobic environment in the runoff area to the anaerobic environment in the stagnant area, their gene abundance had a sensitive response, which can be used as an effective index to identify the stagnant area and the runoff area.

4.5 Relation of C-N-S function genes

Through the above analysis, C-N-S related functional genes are usually enriched in the stagnant zone, indicating that these functional genes were related to each other, as cluster analysis shown in heatmap Fig.11a.

The increased relative abundance of N cycling genes could increase nutrient availability in stagnant coal reservoirs which could in turn affect C metabolism. The C metabolism were also related with each other.

Breakdown of polysaccharides into simple sugars is the primary source of energy and carbon for the microbial community. Degradation pathways for the monosaccharides, glucose, galactose and xylose were also prevalent in the Picrust2 data, include the genes associated with mannose metabolism, carbohydrate hydrolases, lactose and galactose uptake and utilization, L-fructose utilization, xylose utilization (Huang et al., 2017).

In the anaerobic coal reservoir, especially in the stagnant area, inorganic terminal electron acceptors (nitrate, sulfate) are rare, fermentation and acetogenesis are essential pathways for the further degradation of monosaccharides, and supply the substrates for methanogenesis. Fermentation produces low-molecular-weight alcohols and organic acids such as ethanol, propionate, acetate and lactate, as well as hydrogen and carbon dioxide. These genes were particularly abundant in the stagnant area, suggesting increased metabolic substrate production. These substrates such as H_2 and acetic acid could be used by the methanogens, as a result, methanogens were more enriched in stagnant area.

Analysis of these function genes and their abundances and expression enabled us to identify correlations between specific microbial populations and biogeochemistry, and revealed key populations that drive the mineralization of organic matter from polysaccharides through to simple sugars, and the greenhouse gases CO_2 and CH_4.

Fig.10 shows the genes' relative abundance, including C decomposition genes, sulfur metabolism, nitrogen metabolism and methane metabolism. C decomposition genes and nitrogen metabolism genes were more abundant than sulfur metabolism and methane metabolism genes. This suggested fermentation was important in the study area, different microorganisms such as methanogen, nitrate reduction and sulfate reduction bacteria might compete for limited fermentation substrates. The relative low abundance of methanogens was an important reason that biogenic gas was not enriched in the study area. According to the above analysis, the microbial C-N-S cycle pattern in Shizhuangnan Block was built (Fig.13), indicating denitrification, methanogenesis and sulfate reduction, were increased in the stagnant area.

Although the significant increase in abundance of the genes involved in nutrient cycling processes observed in stagnant area may potentially enhance the rates of nutrient cycling, more in-depth studies are necessary to determine the rates and extent of stimulation of different nutrient-cycling processes in the future.

5 Conclusion

(1) The hydrodynamic zone of the study area could be divided into runoff area and stagnant area. They had different hydrodynamic conditions and hydrochemical characteristics. The stagnant area had higher reservoir pressure, gas content and ion concentration than the runoff areas.

Posted on 24 Nov 2022 — CC-BY 4.0 — https://doi.org/10.1002/essoar.10506762.1 — This a preprint and has not been peer reviewed. Data may be preliminary.

(2) The microbial functional community structure was different between runoff area and stagnant area. Genes involved in several important anaerobic respiration processes, such as N cycling genes (e.g., nifDKH, amoB, narGHI, napAB, nirK, norC and nosZ), methanogenesis genes (e.g., mcr, fwd, mtd, mer and mtr) and S cycling genes (e.g., dsrAB, sir, cysN, sat, aprAB and PAPSS), were increased in the stagnant area. The machine learning model shows that these significantly different genes could be used as an effective index to distinguish runoff area and stagnant area.

(3) Increased genes involved in nutrient cycling, including organic matter decomposition, methanogenesis, denitrification and sulfate reduction, contributed to the increase of CO_2 and reduction of sulfate and nitrate from runoff area to stagnant area.

(4) Carbon and hydrogen isotopes indicate that methane in the study area was thermally generated. The main reason for the lack of biogenic methane in the study area was that methanogens were inferior to other anaerobic heterotrophic bacteria in the substrate competition, biogenic methane was consumed by methanotrophic bacteria and was not enough to support the enrichment of a large amount of biogenic methane in the study area.

Acknowledgments

This work was supported by the National Natural Science Foundation of China (grant number 41772159/D0208; grant number 41872178; grant number U1910205). We would like to acknowledge Third Institute of Oceanography (TIO) of the Ministry of Natural Resources for their help in the geochemical test.

Data Availability Statement

All data sources can be downloaded at*http://dx.doi.org/10.17605/OSF.IO/MPA46*.

Reference

Barnhart, E.P., De León, K.B., Ramsay, B.D., Cunningham, A.B., Fields, M.W., 2013. Investigation of coal-associated bacterial and archaeal populations from a diffusive microbial sampler (DMS). International Journal of Coal Geology 115, 64-70.

Evans, P.N., Boyd, J.A., Leu, A.O., Woodcroft, B.J., Parks, D.H., Hugenholtz, P., Tyson, G.W., 2019. An evolving view of methane metabolism in the Archaea. Nat Rev Microbiol 17, 219-232.

Gomes, M.L., Johnston, D.T., 2017. Oxygen and sulfur isotopes in sulfate in modern euxinic systems with implications for evaluating the extent of euxinia in ancient oceans. Geochimica et Cosmochimica Acta 205, 331-359.

Guo, H., Liu, R., Yu, Z., Zhang, H., Yun, J., Li, Y., Liu, X., Pan, J., 2012. Pyrosequencing reveals the dominance of methylotrophic methanogenesis in a coal bed methane reservoir associated with Eastern Ordos Basin in China. International Journal of Coal Geology 93, 56-61.

Guo, H., Yu, Z., Zhang, H., 2015. Phylogenetic diversity of microbial communities associated with coalbed methane gas from Eastern Ordos Basin, China. International Journal of Coal Geology 150-151, 120-126.

Hu, B.L., Shen, L.D., Lian, X., Zhu, Q., Liu, S., Huang, Q., He, Z.F., Geng, S., Cheng, D.Q., Lou, L.P., Xu, X.Y., Zheng, P., He, Y.F., 2014. Evidence for nitrite-dependent anaerobic methane oxidation as a previously overlooked microbial methane sink in wetlands. Proc Natl Acad Sci U S A 111, 4495-4500.

Huang, Z., Sednek, C., Urynowicz, M.A., Guo, H., Wang, Q., Fallgren, P., Jin, S., Jin, Y., Igwe, U., Li, S., 2017. Low carbon renewable natural gas production from coalbeds and implications for carbon capture and storage. Nat Commun 8, 568.

Karlsson, F.H., Tremaroli, V., Nookaew, I., Bergstrom, G., Behre, C.J., Fagerberg, B., Nielsen, J., Backhed, F., 2013. Gut metagenome in European women with normal, impaired and diabetic glucose control. Nature 498, 99-103.

Posted on 24 Nov 2022 — CC-BY 4.0 — https://doi.org/10.1002/essoar.10506762.1 — This a preprint and has not been peer reviewed. Data may be preliminary.

Kuypers, M.M.M., Marchant, H.K., Kartal, B., 2018. The microbial nitrogen-cycling network. Nat Rev Microbiol 16, 263-276.

Li, X., Gilhooly, W.P., Zerkle, A.L., Lyons, T.W., Farquhar, J., Werne, J.P., Varela, R., Scranton, M.I., 2010. Stable sulfur isotopes in the water column of the Cariaco Basin. Geochimica et Cosmochimica Acta 74, 6764-6778.

McCalley, C.K., Woodcroft, B.J., Hodgkins, S.B., Wehr, R.A., Kim, E.H., Mondav, R., Crill, P.M., Chanton, J.P., Rich, V.I., Tyson, G.W., Saleska, S.R., 2014. Methane dynamics regulated by microbial community response to permafrost thaw. Nature 514, 478-481.

Pashin, J.C., McIntyre-Redden, M.R., Mann, S.D., Kopaska-Merkel, D.C., Varonka, M., Orem, W., 2014. Relationships between water and gas chemistry in mature coalbed methane reservoirs of the Black Warrior Basin. International Journal of Coal Geology 126, 92-105.

Schlegel, M.E., McIntosh, J.C., Bates, B.L., Kirk, M.F., Martini, A.M., 2011. Comparison of fluid geochemistry and microbiology of multiple organic-rich reservoirs in the Illinois Basin, USA: Evidence for controls on methanogenesis and microbial transport. Geochimica et Cosmochimica Acta 75, 1903-1919.

Schweitzer, H., Ritter, D., McIntosh, J., Barnhart, E., Cunningham, A.B., Vinson, D., Orem, W., Fields, M.W., 2019. Changes in microbial communities and associated water and gas geochemistry across a sulfate gradient in coal beds: Powder River Basin, USA. Geochimica et Cosmochimica Acta 245, 495-513.

Shen, L.D., Wu, H.S., Gao, Z.Q., Xu, X.H., Chen, T.X., Liu, S., Cheng, H.X., 2015. Occurrence and importance of anaerobic ammonium-oxidising bacteria in vegetable soils. Appl Microbiol Biotechnol 99, 5709-5718.

Subramanian, S., Huq, S., Yatsunenko, T., Haque, R., Mahfuz, M., Alam, M.A., Benezra, A., DeStefano, J., Meier, M.F., Muegge, B.D., Barratt, M.J., VanArendonk, L.G., Zhang, Q., Province, M.A., Petri, W.A., Jr., Ahmed, T., Gordon, J.I., 2014. Persistent gut microbiota immaturity in malnourished Bangladeshi children. Nature 510, 417-421.

Tang, Y.-Q., Ji, P., Lai, G.-L., Chi, C.-Q., Liu, Z.-S., Wu, X.-L., 2012. Diverse microbial community from the coalbeds of the Ordos Basin, China. International Journal of Coal Geology 90-91, 21-33.

Tian, H., Lu, C., Ciais, P., Michalak, A.M., Canadell, J.G., Saikawa, E., Huntzinger, D.N., Gurney, K.R., Sitch, S., Zhang, B., Yang, J., Bousquet, P., Bruhwiler, L., Chen, G., Dlugokencky, E., Friedlingstein, P., Melillo, J., Pan, S., Poulter, B., Prinn, R., Saunois, M., Schwalm, C.R., Wofsy, S.C., 2016. The terrestrial biosphere as a net source of greenhouse gases to the atmosphere. Nature 531, 225-228.

Treude, T., Krause, S., Maltby, J., Dale, A.W., Coffin, R., Hamdan, L.J., 2014. Sulfate reduction and methane oxidation activity below the sulfate-methane transition zone in Alaskan Beaufort Sea continental margin sediments: Implications for deep sulfur cycling. Geochimica et Cosmochimica Acta 144, 217-237.

Wang, B., Sun, F., Tang, D., Zhao, Y., Song, Z., Tao, Y., 2015. Hydrological control rule on coalbed methane enrichment and high yield in FZ Block of Qinshui Basin. Fuel 140, 568-577.

Wang, D.T., Welander, P.V., Ono, S., 2016. Fractionation of the methane isotopologues 13CH4, 12CH3D, and 13CH3D during aerobic oxidation of methane by Methylococcus capsulatus (Bath). Geochimica et Cosmochimica Acta 192, 186-202.

Wang, Q., Guo, H., Wang, H., Urynowicz, M.A., Hu, A., Yu, C.-P., Fallgren, P., Jin, S., Zheng, H., Zeng, R.J., Liu, F., Chen, B., Zhang, R., Huang, Z., 2019. Enhanced production of secondary biogenic coalbed natural gas from a subbituminous coal treated by hydrogen peroxide and its geochemical and microbiological analyses. Fuel 236, 1345-1355.

Wei, M., Yu, Z., Jiang, Z., Zhang, H., 2014. Microbial diversity and biogenic methane potential of a thermogenic-gas coal mine. International Journal of Coal Geology 134-135, 96-107.

Posted on 24 Nov 2022 — CC-BY 4.0 — https://doi.org/10.1002/essoar.10506762.1 — This a preprint and has not been peer reviewed. Data may be preliminary.

Wenk, C.B., Zopfi, J., Blees, J., Veronesi, M., Niemann, H., Lehmann, M.F., 2014. Community N and O isotope fractionation by sulfide-dependent denitrification and anammox in a stratified lacustrine water column. Geochimica et Cosmochimica Acta 125, 551-563.

Wong, H.L., White, R.A., 3rd, Visscher, P.T., Charlesworth, J.C., Vazquez-Campos, X., Burns, B.P., 2018. Disentangling the drivers of functional complexity at the metagenomic level in Shark Bay microbial mat microbiomes. ISME J 12, 2619-2639.

Xu, H., Tang, D., Tang, S., Zhang, W., Meng, Y., Gao, L., Xie, S., Zhao, J., 2015. Geologic and hydrological controls on coal reservoir water production in marine coal-bearing strata: A case study of the Carboniferous Taiyuan Formation in the Liulin area, eastern Ordos Basin, China. Marine and Petroleum Geology 59, 517-526.

Yao, Y., Liu, D., Yan, T., 2014. Geological and hydrogeological controls on the accumulation of coalbed methane in the Weibei field, southeastern Ordos Basin. International Journal of Coal Geology 121, 148-159.

Yatsunenko, T., Rey, F.E., Manary, M.J., Trehan, I., Dominguez-Bello, M.G., Contreras, M., Magris, M., Hidalgo, G., Baldassano, R.N., Anokhin, A.P., Heath, A.C., Warner, B., Reeder, J., Kuczynski, J., Caporaso, J.G., Lozupone, C.A., Lauber, C., Clemente, J.C., Knights, D., Knight, R., Gordon, J.I., 2012. Human gut microbiome viewed across age and geography. Nature 486, 222-227.

Zerkle, A.L., Kamyshny, A., Kump, L.R., Farquhar, J., Oduro, H., Arthur, M.A., 2010. Sulfur cycling in a stratified euxinic lake with moderately high sulfate: Constraints from quadruple S isotopes. Geochimica et Cosmochimica Acta 74, 4953-4970.

Zhang, J., Liang, Y., Yau, P.M., Pandey, R., Harpalani, S., 2015. A metaproteomic approach for identifying proteins in anaerobic bioreactors converting coal to methane. International Journal of Coal Geology 146, 91-103.

Zhang, S., Tang, S., Li, Z., Guo, Q., Pan, Z., 2015. Stable isotope characteristics of CBM co-produced water and implications for CBM development: The example of the Shizhuangnan block in the southern Qinshui Basin, China. Journal of Natural Gas Science and Engineering 27, 1400-1411.

Zhang, S., Tang, S., Li, Z., Pan, Z., Shi, W., 2016. Study of hydrochemical characteristics of CBM co-produced water of the Shizhuangnan Block in the southern Qinshui Basin, China, on its implication of CBM development. International Journal of Coal Geology 159, 169-182.

Zopfi, J., Böttcher, M.E., Jørgensen, B.B., 2008. Biogeochemistry of sulfur and iron in Thioploca-colonized surface sediments in the upwelling area off central chile. Geochimica et Cosmochimica Acta 72, 827-843.

Posted on 24 Nov 2022 — CC-BY 4.0 — https://doi.org/10.1002/essoar.10506762.1 — This a preprint and has not been peer reviewed. Data may be preliminary.

Distribution characteristics of C-N-S microorganism genes in different hydraulic zones of high rank coal reservoirs in southern Qinshui Basin

Wei SHI [a,b,c], Shuheng TANG [a,b,c*], Wenhui HUANG [a,b,c], Songhang ZHANG [a,b,c], Zhongcheng LI [d]

a. MOE Key Lab of Marine Reservoir Evolution and Hydrocarbon Enrichment Mechanism, Beijing 100083, China

b. MOLR Key Lab of Shale Gas Resources Survey and Strategic Evaluation, Beijing 100083，China;

c. School of Energy Resources, China University of Geosciences (Beijing), Beijing 100083, China

d. China United Coalbed Methane Corporation Ltd., Beijing 100011, China

Abstract: Microbial decomposition of carbon and biogenic methane in coal is one of the most important issues in CBM exploration. Microbial C-N-S functional genes in different hydraulic zones of high rank coal reservoirs was studied, demonstrating high sensitivity of this ecosystem to hydrodynamic conditions. The results shows that hydrodynamic strength of the 3# coal reservoir in Shizhuangnan block gradually weakened from east to west, forming the transition feature from runoff area to stagnant area. Compared with runoff area, the stagnant area has higher reservoir pressure, gas content and ion concentrations. The relative abundance of genes associated to C, N and S cycling was increased from the runoff area to stagnant area, including cellulose degrading genes, methane metabolism genes, N cycling genes and S cycling genes. This indicates that the stagnant zone had more active microbial C-N-S cycle. The machine learning model shows that these significantly different genes could be used as effective index to distinguish runoff area and stagnant area. Carbon and hydrogen isotopes indicate that methane in the study area was thermally generated. The methanogens compete with anaerobic heterotrophic bacteria to metabolize limited substrates, resulting in low abundance of methanogens. Meanwhile, the existence of methane oxidizing bacteria suggests biogenic methane was consumed by methanotrophic bacteria, which is the main reason why biogenic methane in the study area was not effectively preserved. In addition, weakened hydrodynamic conditions increased genes involved in nutrient cycling contributed to the increase of CO_2 and consumption of sulfate and nitrate from runoff area to stagnant area.

Keywords: coal bed methane; hydraulic zones; C-N-S microorganisms; genes; coal; water

1 Introduction

Understanding the mechanisms of biospheric characteristics in coal reservoir is important to CBM exploration (Tang et al., 2012; Wei et al., 2014; Guo et al., 2015; Wang et al., 2019). C-N-S microorganisms such as methanogens, nitrifying bacteria, denitrifying bacteria and sulfate reducing bacteria, play an important role in controlling the accumulation of coalbed methane, especially biogenic gas (Guo et al., 2012; Pashin et al., 2014; Schweitzer et al., 2019). Although such microorganisms regulate most biosphere processes related to fluxes of greenhouse gases like CO_2, CH_4 and N_2O, little is known about their role in coal reservoir. Through the systematically collection of water samples from coalbed methane wells in Southern Qinshui Basin for microbial sequencing and geochemical testing, it will show whether microorganisms' distribution changed in different hydrogeochemical zones of the coal seam.

Microorganisms mediate biogeochemical cycles of carbon (C), nitrogen (N), phosphorus (P), sulphur (S) in ecosystem dynamics. Fast developing metagenomic technologies allow us to explore the distribution characteristics and mechanism of microorganisms (Zhang et al., 2015; Wong et al., 2018). Integrated metagenomics technologies such as 16s RNA sequencing was used to determine the microbial community

* Corresponding author, e-mail: tangsh@cugb.edu.cn

structure and functions structure in high rank coal ecosystem in Qinshui Basin.

Environmental factors such as redox conditions, pH, temperature and ion concentrations play an important role in controlling the distribution of various types of microorganisms, especially C-N-S microorganisms (Schlegel et al., 2011; Barnhart et al., 2013). These environmental factors are significantly changed in different hydraulic zones of Southern Qinshui Basin (Zhang et al., 2015). Therefore, this study predicts that hydrological conditions have important controlling effect on C-N-S microorganisms. The aim of this study is to find whether there is shifting microbial function composition from different hydrological zones, such as from runoff area to stagnant area. This study also tries to explain that if different microbial populations in different hydrological zones would have differential geochemical responses and that if weakened hydrodynamic conditions would greatly stimulate the functional genes involved in nutrient-cycling processes.

Southern Qinshui Basin located in north China craton is one of the most highly developed CBM region (Fig.1a) (Wang et al., 2016). Shizhuangnan block, in adjacent to Fanzhuang block and Zhengzhuang block (Fig.1b), is located in the transition area from the southeast edge of the basin to the deep part (Fig.2b). 3# coal seam is the main gas producing layer. The elevation of 3# coal is 223~597m (Fig.2b), and the coal thickness is 4.45~8.75m (Fig.2d). 3# coal seam in the study area has the highest coal rank (R^{o}_{max} 2.92~3.02%) (Fig.2c) and the highest gas content (8~25 m^3/t) in Qinshui Basin (Fig.2a). Now there are more than 1000 drainage wells in this block (Fig.1c). The daily average gas production of 570 drainage wells in Shizhuangnan block was counted and the gas production of most wells exceeded 1000 m^3/d. Moreover, high production wells were mainly distributed in the west of the block (Zhang et al., 2016).

Hydrogeological condition is an important controlling factor of coalbed methane enrichment (Xu et al., 2015; Yao et al., 2014). As the coal bearing strata in the study area are monoclinic structures extending from east to west, the synclines in the west weaken the hydrodynamic strength, the temperature and redox environment of the study area change dramatically from the oxidation runoff belt in the east of the basin edge to the deep stagnant area in the west (Zhang et al., 2015), making it an ideal area to research microbial distribution difference, the hydrogeological conditions of the study area will be introduced below.

2. Geological and hydrogeological conditions

The Qinshui Basin is a Carboniferous-Permian Basin. The outcrops of strata in Qinshui basin include the Cambrian, Ordovician, Permian, Triassic and Quaternary deposits (Fig.1d) (Zhang et al., 2015).

The coal-bearing strata are the Taiyuan and Shanxi Formations in the Upper Pennsylvanian and Lower Permian System (Fig.1e). The outcropping strata in and surrounding Shizhuangnan block include Ordovic Majiagou Group (O_2s), Fengfeng Group (O_2f); Carboniferous Benxi Group (C_2b), Taiyuan Group (C_3t); Permian Shanxi Group (P_1s), Shihezi Group (P_1x, P_2s) and Shiqianfeng Group (P_2sh); Triassic Liujiagou Group (T_1l), Heshanggou Group (T_1h), Ermaying Group (T_2er) and Tongchuan Group (T_2t) and some loose Quaternary layers including Pleistocene (Q_1, Q_2, Q_3) and Holoce (Q_4) (Fig.3a). The adjacent strata exhibit conformity contact, except the O_2f and C_2b, which form a parallel unconformity contact. Shanxi Group consist fine-grained sandstones, coal, carbonates and shale, the average thickness is about 150 m (Fig.1e).

Shizhuangnan block is located in the northwest inclined slope belt of Qinshui Basin. The structure of the study area is striking NNE and dipping the west. The outcrop of the Jinhuo fault on the eastern edge of the basin has a relatively high elevation. Besides, the normal faults developed in the north of the block, including the Sitou Fault, the water blocking fault cuts the coal measure strata and controls the hydrodynamic field in the study area (Zhang et al., 2015).

There are five aquifers in Shizhuangnan block: the Ordovician aquifer, C_3t aquifer, P_1x-P_1s aquifer, T_1l-P_2sh-P_2s aquifer and Quaternary aquifer. The coal seam aquifers are confined by nearly impermeable

mudstones or shales. So generally, the water production rates of 3# coal drainage wells are usually low. However, in the north of study area, faults connect coal reservoir with the roof aquifer, resulting in high water production rates in the north.

The elevation of the #3 coal seam gradually decreases from east to west (Fig.3b). The Jinhuo fault makes the Carboniferous-Permian strata exposed in the eastern part of the study area, where the atmospheric precipitation supplies and seeps from east to west along the monoclinic structure (Fig.3a). Because the Sitou fault in the west of the study area does not conduct water, with the coal seam and sandstone strata extending to the deep, the hydrodynamic conditions gradually weakened, forming the unique hydrogeological conditions of the transition from the east runoff area to the west stagnant area. The syncline in the western stagnant zones is the major high yield area of high production wells, with high salinity, high reservoir pressure and high gas content.

This study focused on the differences of C-N-S function genes between different hydrological zones and the relationship between microbial function structure and geochemical characteristics in the Southern Qinshui Basin. The stable isotopic compositions, major and minor ions in CBM co-produced water, were analyzed, the microbial species in the coal reservoir water at varying depths by 16S rRNA sequencing were investigated to evaluate microbial effects in the Shizhuangnan block.

3. Materials and Methods

3.1. Sample site and collection

A total of 23 CBM co-produced water samples were collected from the CBM wells in Shizhuangnan block in 2019.12, the sample distribution is shown in fig. 4a. All selected CBM wells have been running for more than 5 years constantly and the drainage coal seam is 3# coal. Water samples for ion and isotope analysis and 16S rRNA sequencing were collected directly from the CBM wellhead in 500 mL headspace bottle and 50 mL centrifuge tubes. 0.5 L aluminum foil gas sampling bags were used for gas sampling. During collection, the whole container was filled with the water, placed on the ice, placed in the refrigerator, and immediately sent to the laboratory. All geochemical test including iron test and isotope test were completed in 7 days.

3.2 Ion concentration test

Ion chromatography instrument ICS-1100 (Thermo) was used for the determination of anions and cations. After the water sample was injected into the instrument, it was carried by the eluent and passed through the ion separation column. The conductivity detector was used to measure and record the peak heights of them in turn. From the standard curve drawn under the same conditions, the ion content in water sample could be calculated.

The chromatographic conditions of Cl^-、 NO_2^-、 NO_3^-、SO_4^{2-} were as follows: the column was AG19，4×250 mm; the eluent was KOH, 20 mm; the flow rate was 1 mL/min; the column temperature was 30 ℃. The chromatographic conditions of Na^+、NH_4^+ 、K^+、Mg^{2+}、Ca^{2+} were as follows: the chromatographic column was CS12A，4×250 mm; the eluent was MSA, 20 mm; the flow rate was 1 mL/min; the column temperature was 30 ℃.

3.3 Nitrogen and oxygen isotopes test

To determination nitrogen and oxygen isotope of nitrate. First, the pH value of the water sample was determined. The pH value of water samples was adjusted to be within the pH range of 6~8 by hydrochloric acid (10%) and imidazole solution (2 mol/L). The nitrite was removed in advance with sulfonic acid solution, the amount of sulfonic acid added in the water sample was 1.5 times of that of nitrite, reacted at room temperature for at least 30 min, and then reacted in boiling water bath for 15 min to destroy the generated

complex and eliminate the interference of nitrite.

After the two-step pre analysis, 40 mL of water sample was taken and put it into a 60 ml headspace bottle. 0.8mL of $CdCl_2$ solution (20 g/L), 0.8ml of NH_4Cl solution (250 g/L) and 3×10 cm 4N (or 3N) clean zinc tablet (wiped clean with alcohol) were added and shaken on the shaker at a speed of 220 r/min for 20 min (full reaction). Then the zinc tablet was taken out, the empty bottle was closed to completed the nitrate reduction step. 2 mL of NaN_3 solution (2mol/L) and 1:1 mixture of CH_3COOH (20%) were added into the headspace bottle after nitrate reduction, and shaken violently to mix the sample and reagent. After shaking at 220 r/min for 30 min (full reaction), the azide reaction was ended by adding 1.2 mL NaOH solution (10 mol/L) as the termination agent (the solution was alkaline, which was not conducive to azide reaction).

Nitrate was converted into N_2O gas by the above chemical process reaction, and the nitrogen and oxygen isotope values of N_2O gas were measured by gas bench stable isotope mass spectrometer. The N_2O was carried into Mat 253 isotope ratio mass spectrometer to determine the nitrogen isotope ratio.

3.4 Water hydrogen and oxygen isotopes test

The hydrogen and oxygen isotopic composition of water was determined by Gasbench II-IRMS continuous flow. The constant temperature sample tray temperature was 28 ℃, the poraplot Q chromatographic column temperature was 70 ℃, and the He pressure was 120 kPa.

For δD-H_2O analysis, the water sample was packaged in a 2mL chromatographic bottle, covered with a hollow cap and placed on the sample rack. Hydrogen isotope in water was measured by high temperature pyrolysis method. The flow rate of carrier gas He was 100 mL/min, the temperature of reaction tube was 1380 ℃, and the furnace temperature was 75 ℃. Then the hydrogen isotope was measured by Delta V advantage isotope mass spectrometer. The calibration curves of hydrogen isotopes in water were established by inserting standard samples with different abundances before and after the samples.

For $\delta^{18}O$-H_2O analysis, 200 μL water sample and standard water were taken and put into a 12 mL (labco) reaction bottle, and the cap was tightened. Then the air blowing needle was fixed, the working procedure of the automatic sampler was set, 0.3% of CO_2 + He mixture was filled in and inflated for 5 minutes to take the air from the bottle. After the completion of the filling, the water sample was kept in equilibrium for 18 hours, so that it could reach the equilibrium of isotope exchange. The CO_2 isotope ratio after the equilibrium of isotopic fractionation was determined by Delta V advantage isotope mass spectrometer with fixed injection needle.

3.5 DIC carbon isotope test

For one sample, 8 drops of anhydrous phosphoric acid was added to the 12 mL sample bottle (labco) and the bottle was put on the constant temperature sample disk in sequence. The air blowing needle was fixed, the working procedure of GC PAL automatic sampler was set, and the sample bottle was successively emptied with helium for 5min to remove the influence of the air in the bottle on the determination of C isotope ratio. 0.2mL water sample was added into the sample bottle, reacted at 45 °C on the dry heater for 45 minutes, and centrifugated before sample measurement.

The mixture of high purity helium and CO_2 was separated from other impurities by gas chromatography at 75 ℃. The separated CO_2 is carried into Delta V detector by helium, and ionized by high-energy electron beam. After accelerated electric field, gaseous ions with different mass charge ratios (m/z44, m/z45, m/z46) enter the magnetic field to separate into different ion beams, which enter the receiver and convert them into electrical signals to determine the carbon isotope ratio. The accuracy of $\delta^{13}C_{DIC}$ value is ± 0.08 ‰.

3.6 Methane isotope test

The instrument used in methane and carbon dioxide isotope analysis was the on-line analysis and test system (GC/C/IRMS) produced by ThermrFinnigan company, it mainly composed of Trace Ultra

Chromatograph, combustion furnace (GC Combustion III) and stable isotope mass spectrometer Delta V Advantage. The mass spectrometry test conditions were set as follows: ion source high pressure was 3.0 kv, ion source emission current was 1.5 mA. The chromatography conditions were set as follows: Poraplot Q capillary column (27 m×0.32 mm×20.00 μm) was chosen as chromatographic column, high purity He (99.999%) was used as carrier gas, column flow rate was 1.5 mL/min, sample inlet temperature was 120 ℃.

For $\delta^{13}C$-CH_4 analysis, the temperature of the oxidation furnace (NiO/ CuO/ PI) was 960 ℃ and the temperature of the reduction furnace was 640 ℃. Then methane was oxidized into carbon dioxide gas in combustion furnace, and then introduced into isotope mass spectrometer to detect carbon isotope value.

For δD-CH_4 analysis, the carrier gas was helium (1.2 mL/min), the split ratio was between 1:8 and 1:40 depending on methane concentration, and the temperatures of the GC oven and injector were 40°C and 200°C, respectively. Analysis of δD-CH_4 involved on-line transfer of samples from a high temperature conversion reactor (containing an empty ceramic tube covered with graphite layer that was kept at a temperature of 1440°C) in which compounds were pyrolyzed to molecular hydrogen, carbon, and carbon monoxide, prior to their transfer into the mass spectrometer via a ConfloIV interface. Then molecular hydrogen was introduced into isotope mass spectrometer to detect hydrogen isotope value.

3.7 Gene extraction, PCR amplicon, and sequencing analysis

Water samples obtained from the CBM well for gene sequencing were stored in an incubator filled with dry ice under a low temperature condition (0℃) while being transferred to the laboratory. The DNA for each sample was extracted with FastDNA SPIN Kit (MP Biomedicals). DNAs were measured by PicoGreen dsDNA Assay Kit (Life Technologies) and subsequently diluted to 3.5 ng/μl. The V3-V4 region of the bacterial 16S rRNA gene was amplified by degenerate PCR primers 341F: CCTACGGGNGGCWGCAG and 805R: GACTACHVGGGTATCTAATCC. Each sample was amplified in triplicate (together with water control) in a 30 μl reaction system, which contained 3 μl of diluted DNA, 0.75 U PrimeSTAR HS DNA polymerase, 1 x PrimSTAR buffer (Takara), 0.2 mM deoxyribonucleoside triphosphates (dNTPs) and 10 pM of barcoded forward and reverse primers. After an initial denaturation step at 98 ℃ for 30 s, the targeted region was amplified by 25 cycles of 98 ℃ for 10 s, 55 ℃ for 15 s and 72 ℃ for 60 s, followed by a final elongation step of 5 min at 72 ℃. If there was no visible amplification from negative control (no template added), triplicate PCR products were mixed and purified using an AMPure XP Kit (Beckman Coulter). The purified PCR products were measured by Nanodrop (NanoDrop 2000C, Thermo Scientific), and diluted to 10 ng/μl as templates for the second step of the PCR. All samples were amplified in triplicate with second-step primers, using identical conditions to the first step of the PCR but with eight cycles.

Technical replicates of each sample were combined and run on a 1.2% (w/v) agarose gel, and the bacterial 16S rRNA gene amplicons were extracted using a QIAquick Gel Extraction Kit (Qiagen). DNAs were subsequently measured with a PicoGreen dsDNA Assay Kit (Life Technologies) and 10 ng of each sample were mixed. Final amplicon libraries were purified twice using a Agencourt AMPure XP Kit (Beckman Coulter) and subjected to a single sequencing run on the HiSeq 2500 platform (Illumina Inc).

Bioinformatics analysis on 16S rRNA gene profiling. The 16S rRNA gene sequences were processed using QIIME v.1.9.1 and USEARCH v.10.0. The quality of the paired-end Illumina reads was checked by FastQC v.0.11.5 and processed in the following steps by USEARCH: joining of paired-end reads and relabeling of sequencing names; removal of barcodes and primers; filtering of low-quality reads; and finding non-redundancy reads.

Unique reads were clustered into OTUs with 97% similarity. OTUs were aligned to the SILVA database to remove sequences from chimera. The OTU table was generated by USEARCH. The taxonomy of the

representative sequences was classified with the RDP classifier. Functional annotations of prokaryotic taxa were carried out using Picrust2 against the KEGG databases.

Three complementary non-parametric multivariate analyses, non-parametric multivariate analysis of variance (Adonis), analysis of similarity (ANOSIM), and the multi-response permutation procedure (MRPP;), were used to test the differences in soil microbial communities between warming and control treatments. The difference of the C-N-S function genes was detected by Welch's t-test with FDR correction in STAMP. The heatmaps were drawn by the "pheatmap" package.

A maximum likelihood phylogeny of main C-N-S microbes was generated from the aligned RDP sequence using Iqtree. All phylogenetic trees were edited in Itol.

To acquire the best discriminant performance of C-N-S microbes across runoff and stagnant area, we classified the abundances of bacterial taxa using the "randomForest" package. Cross-validation was performed by the rfcv function for selecting appropriate features. The varImpPlot function was used to show the importance of features in the classification.

4 Results and discussion

4.1 Geochemical results

Geochemical composition of CBM co-produced water is useful to identify hydraulic zone as water and rock interact along the flow paths. CBM co-produced water usually contained several important ions, with Na^+, K^+, Ca^{2+}, Fe^{3+}, Mg^{2+}, Cl^-, HCO_3^-, CO_3^{2-}, NO_3^- and SO_4^{2-} accounting for most of the total solute in groundwater. Generally, shallow coal seam water in runoff area was characterized with lower KDS and higher Fe^{3+}, NO_3^- and SO_4^{2-} contents, whereas deep coal seam water in stagnant area was characterized with higher KDS contents and lower Fe^{3+}, NO_3^- and SO_4^{2-} contents.

The concentrations of Na^+ (K^+) in the water samples ranged from 241 to 1187 mg/L, whereas the concentrations of Cl^- ranged from 35 to 1609 mg/L. The concentrations of Ca^{2+} in the CBM co-produced water ranged from 0.12 to 10.7 mg/L. The concentrations of Mg^{2+} ranged from 0.57 to 4.31 mg/L. Dissolution of halite (NaCl) or sylvite (KCl) is the main source of Na^+ or K^+ in coal reservoir water. Additionally, silicates weathering could release Na^+ or K^+, respectively. Cation exchange between Ca^{2+} or Mg^{2+} and Na^+ or K^+ can increase content of Na^+ and K^+ by reducing Ca^{2+} or Mg^{2+}. The water rock reaction in the stagnant area was more sufficient, which led to the increase of mineralization (KDS) in the stagnant area.

In contract, NO_3^-, SO_4^{2-} and Fe^{3+} were more abundent in the runoff area, they are anaerobic electron acceptors closely realted to anaerobic respiration of microorganisms. The concentrations of NO_3^- ranged from 0.24 to 1.01 mg/L. The concentrations of SO_4^{2-} ranged from 6.93 to 17.02 mg/L. The concentrations of Fe^{3+} ranged from 0.3 to 5.57 mg/L.

The hydrogen and oxygen isotope composition of water could be used to identify the groundwater source. The following equation of atmospheric precipitation line in China was adopted: $\delta D = 7.9\delta^{18}O+8.2$. According to Fig. 7a, the water samples taken were distributed near the atmospheric precipitation line, indicating that the source of coal seam water is predominantly atmospheric precipitation.

The value of $\delta^{13}C_{CH4}$ ranged from -20 to -40‰ and δD ranged from -270 to -130‰, both the methane gas samples and soluble methane samples suggested methane in the study area is thermogenic origin (Fig. 7b).

The value of $\delta^{15}N_{NO3}$ ranged from -1 to -10‰ and $\delta^{18}O_{NO3}$ ranged from -6 to -7‰, suggesting the nitrate may come from biological nitrogen fixation or nitrification of NH_4^+ fertilizer on the ground (Fig. 7c).

4.2 Division of runoff area and stagnant area

The sampling was mainly in the south of Shizhuangnan block with the purpose of comparing the distribution differences of C-N-S functional genes between stagnant area and runoff area, so one of the

most import issues in this study was to divide different hydrodynamic zones. Sever factors that change significantly were considered, as shown in the contour map.

The direct manifestation of hydrodynamic field is water pressure, so the three-dimensional hydrodynamic field in the sampling area was firstly modeled, and clearly the the water pressure rose sharply from east to the west on the edge of the western syncline (Fig. 5b), which was caused by the convergence of water flow in the low-lying area of the western stagnant area due to the Sitou fault which blocked water at the boundary.

The edge of the syncline in the west of the study area could be used as the boundary line to divide the hydrodynamic zones, as indicated by the black dotted line (Fig.4). Through this boundary, the atmospheric precipitation transit from the flowing state to the stagnant state, that was, from the runoff area to the stagnant area. The stagnant environment was conducive to the enrichment and preservation of coalbed methane. Indeed, the measured gas content had obvious changed across this line, from 7~12 m^3/t to 14~20 m^3/t (Fig.4). The stagnant environment made the interaction between water and rock stronger, resulting in higher mineralization in the stagnant area, which was also confirmed by the KDS concentration, as shown in the Fig. 6d. As there was transition from oxidation environment in runoff area to reduction environment in stagnant area, the geochemical data also support the above view, the concentration of NO_3^-, SO_4^{2-} , Fe^{3+} and $\delta^{13}C_{DIC}$, had obvious changed on both sides of this line, NO_3^-, SO_4^{2-} and Fe^{3+} were anaerobic electron acceptor in involved in several important anaerobic respiration processes, such as denitrification, sulfate reduction and iron reduction, their concentration were all reduced in the stagnant area's anoxic environment , shown in Fig. 6a~6c.

It could be predicted that with the precipitation moving from east to west, the dissolved oxygen in water was gradually consumed, the aerobic respiration was weakened while the anaerobic respiration was enhanced, resulting in the consumption of anaerobic electron acceptors, such as NO_3^-, SO_4^{2-} and Fe^{3+} in the stagnant area. As the environment in the stagnant area was lack of oxygen supply, the anaerobic respiration was stronger than that in the runoff area, and the consumption of the electron acceptors was stronger in stagnant area.

Anaerobic respiration such as methanogenesis has isotope fractionation effect (Wang et al., 2016), resulting biogenic methane enriches lighter carbon and then aggravates dissolved inorganic carbon isotope (McCalley et al., 2014). If the methane production in stagnant area was stronger, the dissolved inorganic carbon isotope in stagnant area would be more positive than that in runoff area. The dissolved inorganic carbon isotope test results supported this view the C pool was isotopically fractionated by microbial methanogenesis or other microbial carbon cycling effect(Fig.6e).

Considering the structural location (Fig.6f), water pressure (Fig.5b), gas content (Fig.4) and geochemical data (Fig. 6a~6e), the edge of syncline structure was selected as the boundary of dividing runoff area and stagnant area, as shown in Fig.5a, the red area was stagnant area, the blue area was runoff area, and the gray area in the north was fault developed deep coal.

In general, the structural location determined the hydrodynamic conditions, and then affected the distribution of hydrochemical field. This study pedicteded that the microbial functional genes involved anaerobic respiration such as denitrification, sulfate reduction were stronger in stagnant area. Next, this prediction would be proved by the gene sequencing results.

4.3 Microbial community functional structure

For the 23 water samples collected from CBM wells, 5 samples located in the runoff areas and 18 samples in the stagnant areas (Fig.5a). We generated a bacterial community profile for each sample via PCR amplification of the 16S ribosomal RNA (rRNA) gene targeting regions V3-V4 using primers 341F

and 805R, followed by Illumina sequencing. 1966435 high-quality sequences from 23 samples were obtained (average, 85497; range, 53843-147971 reads per sample). High quality reads were analyzed with USEARCH, removing chimeric and organelle sequences, to produce 8264 operational taxonomic units (OTUs).

In all the samples, at the class level, Gammaproteobacteria, Betaproteobacteria, Deltaproteobacteria and Alphaproteobacteria were the most abundant bacteria, made up more than 85% of all microorganisms. Clostridia, Bacteroidia, Flavobacteriia, Bacilli, Methanobacteria, Actinobacteria were also present at higher relative abundance, but much lower than the four most abundant classes (Fig.8a).

90 most highly abundant microorganisms related to methanogenesis, denitrification, sulfate reduction and methane oxidation were selected. Maximum likelihood phylogenetic was constructed based on 16s V3-V4 sequences, shown in Fig.8b. There were three orders of Methanogens in study area, including Methanobacteriales, Methanomicrobiales and Methanosarcinales. Methane oxidizing bacteria included Methylococcales and Methylophilales. Denitrifying bacteria included Burkholderiales and Rhodobacterales. Sulfate reduction bacteria included Desulfobacterales and Desulfovibrionales. Aerobic ammonia oxidation bacteria (AOB) included Nitrosomonadales. Nitrification bacteria included Nitrospirales and Nitrosomonadales. The order of anammox bacteria was belonged to Candidatus Brocadiales.

Consistent with this expectation, the microbial community functional gene structure was different between runoff area and stagnant area. All of the nonparametric multivariate statistical tests of dissimilarity (MRPP, ANOSIM, and Adonis) showed that the overall functional structure of 3# coal production water's microbial communities was different between runoff area and stagnant area ($p < 0.005$, Table 1). Cluster analysis of C-N-S function genes showed that the samples from runoff area and stagnant area were completely clustered into two groups, which further indicated the functional differences of microorganisms between the two groups (Fig.11a).

The relative abundance of genes associated to C, N and S cycling was increased from the runoff area to stagnant area (Fig. 9). In contrast, only few functional genes, which mainly belong to functions related to assimilatory nitrate reduction, were significantly ($p < 0.005$) decreased in relative abundance in the stagnant area. Next, it will be discussed in detail.

4.3.1 C cycling

Changes in hydrodynamic conditions from runoff area to stagnant area significantly impacted a number of microbial functional groups important for C decomposition. 25 genes associated with decomposition of labile or recalcitrant C were detected. Among them, 9 genes exhibited higher relative abundance in stagnant area than runoff area samples ($p < 0.05$, Fig. 9a), including cellulose 1,4-beta-cellobiosidase (P = 2.64E-07), licheninase (P = 5.03E-06), alpha-mannosidase (P = 8.89E-05), 6-phospho-beta-glucosidase (P = 0.000490162), alpha-glucuronidase (P = 0.000582225), endo-1,4-beta-galactosidase (P = 0.000920978), endoglucanase (P = 0.002333825), chitinase (P = 0.002343304), beta-mannosidase (P = 0.018552947). Increases of the genes involved in recalcitrant C decomposition suggested the possible degradation of old recalcitrant C in stagnant area.

This study held the idea that these recalcitrant C came from the plant debris on the ground. With the atmospheric precipitation moving from the eastern outcrop to the western stagnant environment in the study area, the temperature and pressure in the stagnant area were increased from the runoff area, which is more favorable for the degradation of recalcitrant C. The relative abundance of recalcitrant C decomposition genes was more than that of methanogenesis genes. In the case that the high rank coal in the study area was difficult to be degraded, the degradation of recalcitrant C from the surface would be an important substrate for microorganisms, and the monosaccharide produced could further provide substrates

for other carbohydrate metabolism. As genes associated with mannose metabolism, carbohydrate hydrolases, lactose and galactose uptake and utilization, L-fructose utilization, xylose utilization and chitin utilization were all increased in the stagnant area (Supplementary Fig. 1). Overall, as these functional genes directly participate in C degradation, their higher abundance could enhance C decomposition and enhance methanogenesis and other anaerobic heterotrophic microorganisms such as nitrate reducing bacteria and sulfate reducing bacteria.

4.3.2 Methane metabolism

For all the methanogenesis genes resulted in Picrust2 analysis, the relative abundance of methanogenesis genes were increased from runoff area to stagnant area (Fig.9d), including mcrA, mcrB, mcrG, the key enzyme in all types of methanogenesis ($p < 0.00005$). FwdA-FwdH ($p < 0.00001$), mtd ($p < 0.00002$), mer ($p < 0.000002$), mtrA-mtrH ($p < 0.00002$), MvhADG–HdrABC ($p < 0.05$) in hydrogenotrophic methanogenesis showed more relative abundance in stagnant area too. Codh–Acs ($p < 0.00007$) in aceticlastic methanogenesis and MtaA-MtaC ($p < 0.00008$) in methylotrophic methanogenesis were also more abundant in stagnant area. What's more, fbiC ($p < 0.03$), cofH, cofG, cofC, cofD and cofE ($p < 0.0006$) in F_{420} biosynthesis, mfnB, mfnD, mfnE, mfnF ($p < 0.02$) in methanofuran biosynthesis and comC, comE, comD ($p < 0.00002$) in Coenzyme M biosynthesis were increased in the stagnant area. Suggesting an increase of all types of methanogenesis in the western stagnant area.

In both the runoff area and stagnant area samples there was a greater relative abundance of pmoB (a gene encoding particulate methane monooxygenase subunit B) than any methanogenesis genes, suggesting that of the biogenic methane could be oxidized aerobically (Treude et al., 2014). Indeed, the exploitation of CBM wells, including drilling and hydraulic fracturing, increased the opening degree and oxygen content of the coal seam, resulting in a high relative abundance of methane oxidizing bacteria in the samples. These aerobic bacteria grew in the wellbore or drainage outlet, consuming the dissolved methane of the produced water, which explained why there was methanogenesis microorganisms in the study area, but biogenic methane had not been effectively preserved. The aerobic and anaerobic oxidation of methane might have an important consumption mechanism of biogenic gas in the process of CBM generation history, although anaerobic methane oxidizing bacteria (ANME and M. oxyfera) were not detected in the 16S sequencing of our recently collected water samples.

Because the isotope characteristics of both the methane gas samples and the water-soluble methane samples showed complete thermogenic (Fig.7b), there were two possibilities that biogenic gas does not exist: (1) In most of the historical methane generation process, due to the unsuitable temperature and pressure conditions, methanogens did not exist or exist in the low abundance. The methanogens began to grow only when the outcrop of uplifted coal seams received meteoric water supply of organic matter and minerals. (2) In the gas generation stage of coalbed methane, the existence of methanogens was accompanied by aerobic and anaerobic oxidation methylotrophic bacteria, and biogenic methane was consumed by these microorganisms (Evans et al., 2019). In addition, because methanogens and sulfate reducing bacteria shared the same substrate H_2, this competition mechanism further compressed the living space of methanogens, resulting in that biogenic methane is not rich in the study area.

4.3.3 N cycling

Nitrogen, including nitrate, nitrite and ammonium, is an important element for all microorganisms and is required for the biosynthesis of key cellular components such as amino acid and nucleotide (Wenk et al., 2014; Kuypers et al., 2018; Tian et al., 2016; Shen et al., 2015; Hu et al., 2014). 25 genes associated with N cycling were detected, including nitrogen fixation, anaerobic oxidation of ammonia, nitrification, anammox, dissimilatory nitrate reduction, assimilatory nitrate reduction and denitrification. There were also different

genes involved in N cycling between runoff area and stagnant area (Fig. 9b), Most (56%) of the Picrust2-detected functional genes involved in N cycling were increased from runoff area to stagnant area ($p < 0.05$; Fig. 9b), consistent with the previous prediction that weakened hydrodynamic conditions enhances nutrient cycling.

For example, the abundance of N_2-fixing genes was higher in response to hydrodynamic conditions ($p < 0.05$; Fig. 9b), the nifD ($p = 0.00007$), nifH ($p = 0.0001$), nifK ($p = 0.0007$) had higher abundance in the stagnant samples. In addition, weakened hydrodynamic strength from runoff area to stagnant area seemed to decrease dissimilatory nitrate reduction and increase nitrification, denitrification processes, as indicated by decreased narG ($p = 0.017$), narH ($p = 0.02$), narI ($p = 0.01$) gene, and increased nirK ($p = 0.008$), nosZ ($p = 0.00002$), norC ($p = 0.001$), napA ($p = 0.0008$), napB ($p = 0.0005$), nrfA ($p = 0.000004$), and amoB ($p = 0.04$) gene from runoff area to stagnant area (Fig. 9b). The increase in nitrification gene amoB and N_2-fixing gene nifDH would lead to higher nitrite and nitrate concentrations, which was also supported by the greater abundance of genes for various reductive processes which used nitrate as an electron acceptor, such as nirK, nosZ, norC for denitrification, nrfA for dissimilatory nitrate reduction to ammonium (narG, narH, narI, napA, napB shared by denitrification and dissimilatory nitrate reduction) and nirA for assimilatory nitrate reduction (Fig. 9b). Significant different N-cycle related genes between the two groups were labeled on the N pathway map, as shown in Fig.11b.

Almost all the N cycling genes were more abundant in the stagnant area, except dissimilatory nitrate reduction, were more abundant in the runoff area. This was possible, as NO_3^- concentration decreased from runoff area to stagnant area, suggesting the consumption of nitrate in runoff area by the first step of dissimilatory nitrate reduction. Reduction products such as nitrite would continue to converge into the stagnant area, and then be reduced by denitrification microorganisms, resulting in the increase of denitrification genes, such as nirK, norC and nosZ. The increased relative abundance of N cycling genes (N fixation and nitrification) and other nutrient-cycling genes could increase nutrient (especially N) availability in stagnant coal reservoirs, which is important for ecosystem C dynamics because N is a limiting factor for microorganism growth in most groundwater ecosystems. The enhanced N uptake could in turn affect C metabolism such as cellulose, mannose metabolism, carbohydrate metabolism, which increased in response to hydrodynamic conditions.

As the nitrogen and oxygen isotopes of nitrate shows that nitrate may come from surface soil and fertilizer (Fig. 7c), which seep into stagnant area with meteoric water, some nitrate may also come from the nitrogen fixation and of in-situ microorganisms in coal seam itself.

4.3.4 S cycling

Sulfur metabolism in microorganisms consists of redox reactions of organic and inorganic sulfur substrates that can play a major part in the biogeochemical cycle (Zerkle et al., 2010; Zopfi et al., 2008; Li et al., 2010; Treude et al., 2014; Gomes et al., 2017). As the same of denitrification, sulfate reduction is an anaerobic respiration that might be stronger in stagnant area. Nine of the fourteen detected sulfur metabolic genes had higher relative abundance in stagnant area than in runoff area (Fig.9c), suggesting enhanced microbial functional capacity for S cycling in stagnant area. These genes included dsrAB encoding dissimilatory sulfite reductase ($p < 0.001$), sir encoding sulfate reductase ($p = 0.003$), cysN encoding sulfate adenylyltransferase ($p = 0.008$), sat encoding sulfate adenylyltransferase ($p = 0.00008$), aprAB encoding adenylylsulfate reductase ($p < 0.02$) and PAPSS encoding 3'-phosphoadenosine 5'-phosphosulfate synthase ($p = 0.03$).

4.4 Machine-learning classification C-N-S genes between runoff area and stagnant area

As C-N-S genes changed significantly between runoff area and stagnant area, they could be used as biomarkers to differentiate water samples of runoff area and stagnant area. The prediction model was established using a random-forest machine-learning method to correlate runoff area and stagnant area with Picrut2 data (Subramanian et al., 2014; Yatsunenko et al., 2014; Karlsson et al., 2014). Ten-fold cross-validation with five repeats was carried out to evaluate the importance of indicator bacterial families. The crossvalidation error curve stabilized when the most relevant genes were used (Fig.12b). These genes included methanogenesis genes (mtr, fwd, mcr, mtd, mtr, hdr, mer and mvh); aceticlastic methanogenesis gene (cdh); F_{420} biosynthesis gene (cof); Coenzyme M biosynthesis gene(com); dissimilatory and assimilatory sulfate reduction genes (sat, sir, dsr and apr); assimilatory nitrate reduction genes (napA and nrfA) and denitrification gene (nosz). Fig.12a showed the above-mentioned functional genes' relative abundence in runoff area samples and stagnant area samples. This consisted with the Welch's t-test results. As these function genes related to methanogenesis, nitrate reduction and sulfate reduction were all anaerobic respiration genes, when the hydrogeological environment transits from the aerobic environment in the runoff area to the anaerobic environment in the stagnant area, their gene abundance had a sensitive response, which can be used as an effective index to identify the stagnant area and the runoff area.

4.5 Relation of C-N-S function genes

Through the above analysis, C-N-S related functional genes are usually enriched in the stagnant zone, indicating that these functional genes were related to each other, as cluster analysis shown in heatmap Fig.11a.

The increased relative abundance of N cycling genes could increase nutrient availability in stagnant coal reservoirs which could in turn affect C metabolism. The C metabolism were also related with each other.

Breakdown of polysaccharides into simple sugars is the primary source of energy and carbon for the microbial community. Degradation pathways for the monosaccharides, glucose, galactose and xylose were also prevalent in the Picrust2 data, include the genes associated with mannose metabolism, carbohydrate hydrolases, lactose and galactose uptake and utilization, L-fructose utilization, xylose utilization (Huang et al., 2017).

In the anaerobic coal reservoir, especially in the stagnant area, inorganic terminal electron acceptors (nitrate, sulfate) are rare, fermentation and acetogenesis are essential pathways for the further degradation of monosaccharides, and supply the substrates for methanogenesis. Fermentation produces low-molecular-weight alcohols and organic acids such as ethanol, propionate, acetate and lactate, as well as hydrogen and carbon dioxide. These genes were particularly abundant in the stagnant area, suggesting increased metabolic substrate production. These substrates such as H_2 and acetic acid could be used by the methanogens, as a result, methanogens were more enriched in stagnant area.

Analysis of these function genes and their abundances and expression enabled us to identify correlations between specific microbial populations and biogeochemistry, and revealed key populations that drive the mineralization of organic matter from polysaccharides through to simple sugars, and the greenhouse gases CO_2 and CH_4.

Fig.10 shows the genes' relative abundance, including C decomposition genes, sulfur metabolism, nitrogen metabolism and methane metabolism. C decomposition genes and nitrogen metabolism genes were more abundant than sulfur metabolism and methane metabolism genes. This suggested fermentation was important in the study area, different microorganisms such as methanogen, nitrate reduction and sulfate reduction bacteria might compete for limited fermentation substrates. The relative low abundance of methanogens was an important reason that biogenic gas was not enriched in the study area. According to the above analysis, the microbial C-N-S cycle pattern in Shizhuangnan Block was built (Fig.13), indicating

denitrification, methanogenesis and sulfate reduction, were increased in the stagnant area.

Although the significant increase in abundance of the genes involved in nutrient cycling processes observed in stagnant area may potentially enhance the rates of nutrient cycling, more in-depth studies are necessary to determine the rates and extent of stimulation of different nutrient-cycling processes in the future.

5 Conclusion

(1) The hydrodynamic zone of the study area could be divided into runoff area and stagnant area. They had different hydrodynamic conditions and hydrochemical characteristics. The stagnant area had higher reservoir pressure, gas content and ion concentration than the runoff areas.

(2) The microbial functional community structure was different between runoff area and stagnant area. Genes involved in several important anaerobic respiration processes, such as N cycling genes (e.g., nifDKH, amoB, narGHI, napAB, nirK, norC and nosZ), methanogenesis genes (e.g., mcr, fwd, mtd, mer and mtr) and S cycling genes (e.g., dsrAB, sir, cysN, sat, aprAB and PAPSS), were increased in the stagnant area. The machine learning model shows that these significantly different genes could be used as an effective index to distinguish runoff area and stagnant area.

(3) Increased genes involved in nutrient cycling, including organic matter decomposition, methanogenesis, denitrification and sulfate reduction, contributed to the increase of CO_2 and reduction of sulfate and nitrate from runoff area to stagnant area.

(4) Carbon and hydrogen isotopes indicate that methane in the study area was thermally generated. The main reason for the lack of biogenic methane in the study area was that methanogens were inferior to other anaerobic heterotrophic bacteria in the substrate competition, biogenic methane was consumed by methanotrophic bacteria and was not enough to support the enrichment of a large amount of biogenic methane in the study area.

Acknowledgments

This work was supported by the National Natural Science Foundation of China (grant number 41772159/D0208; grant number 41872178; grant number U1910205). We would like to acknowledge Third Institute of Oceanography (TIO) of the Ministry of Natural Resources for their help in the geochemical test.

Data Availability Statement

All data sources can be downloaded at http://dx.doi.org/10.17605/OSF.IO/MPA46.

Reference

Barnhart, E.P., De León, K.B., Ramsay, B.D., Cunningham, A.B., Fields, M.W., 2013. Investigation of coal-associated bacterial and archaeal populations from a diffusive microbial sampler (DMS). International Journal of Coal Geology 115, 64-70.

Evans, P.N., Boyd, J.A., Leu, A.O., Woodcroft, B.J., Parks, D.H., Hugenholtz, P., Tyson, G.W., 2019. An evolving view of methane metabolism in the Archaea. Nat Rev Microbiol 17, 219-232.

Gomes, M.L., Johnston, D.T., 2017. Oxygen and sulfur isotopes in sulfate in modern euxinic systems with implications for evaluating the extent of euxinia in ancient oceans. Geochimica et Cosmochimica Acta 205, 331-359.

Guo, H., Liu, R., Yu, Z., Zhang, H., Yun, J., Li, Y., Liu, X., Pan, J., 2012. Pyrosequencing reveals the dominance of methylotrophic methanogenesis in a coal bed methane reservoir associated with Eastern Ordos Basin in China. International Journal of Coal Geology 93, 56-61.

Guo, H., Yu, Z., Zhang, H., 2015. Phylogenetic diversity of microbial communities associated with coalbed methane gas from Eastern Ordos Basin, China. International Journal of Coal Geology 150-151, 120-126.

Hu, B.L., Shen, L.D., Lian, X., Zhu, Q., Liu, S., Huang, Q., He, Z.F., Geng, S., Cheng, D.Q., Lou, L.P., Xu, X.Y., Zheng, P., He, Y.F., 2014. Evidence for nitrite-dependent anaerobic methane oxidation as a previously overlooked microbial methane sink in wetlands. Proc Natl Acad Sci U S A 111, 4495-4500.

Huang, Z., Sednek, C., Urynowicz, M.A., Guo, H., Wang, Q., Fallgren, P., Jin, S., Jin, Y., Igwe, U., Li, S., 2017. Low carbon renewable natural gas production from coalbeds and implications for carbon capture and storage. Nat Commun 8, 568.

Karlsson, F.H., Tremaroli, V., Nookaew, I., Bergstrom, G., Behre, C.J., Fagerberg, B., Nielsen, J., Backhed, F., 2013. Gut metagenome in European women with normal, impaired and diabetic glucose control. Nature 498, 99-103.

Kuypers, M.M.M., Marchant, H.K., Kartal, B., 2018. The microbial nitrogen-cycling network. Nat Rev Microbiol 16, 263-276.

Li, X., Gilhooly, W.P., Zerkle, A.L., Lyons, T.W., Farquhar, J., Werne, J.P., Varela, R., Scranton, M.I., 2010. Stable sulfur isotopes in the water column of the Cariaco Basin. Geochimica et Cosmochimica Acta 74, 6764-6778.

McCalley, C.K., Woodcroft, B.J., Hodgkins, S.B., Wehr, R.A., Kim, E.H., Mondav, R., Crill, P.M., Chanton, J.P., Rich, V.I., Tyson, G.W., Saleska, S.R., 2014. Methane dynamics regulated by microbial community response to permafrost thaw. Nature 514, 478-481.

Pashin, J.C., McIntyre-Redden, M.R., Mann, S.D., Kopaska-Merkel, D.C., Varonka, M., Orem, W., 2014. Relationships between water and gas chemistry in mature coalbed methane reservoirs of the Black Warrior Basin. International Journal of Coal Geology 126, 92-105.

Schlegel, M.E., McIntosh, J.C., Bates, B.L., Kirk, M.F., Martini, A.M., 2011. Comparison of fluid geochemistry and microbiology of multiple organic-rich reservoirs in the Illinois Basin, USA: Evidence for controls on methanogenesis and microbial transport. Geochimica et Cosmochimica Acta 75, 1903-1919.

Schweitzer, H., Ritter, D., McIntosh, J., Barnhart, E., Cunningham, A.B., Vinson, D., Orem, W., Fields, M.W., 2019. Changes in microbial communities and associated water and gas geochemistry across a sulfate gradient in coal beds: Powder River Basin, USA. Geochimica et Cosmochimica Acta 245, 495-513.

Shen, L.D., Wu, H.S., Gao, Z.Q., Xu, X.H., Chen, T.X., Liu, S., Cheng, H.X., 2015. Occurrence and importance of anaerobic ammonium-oxidising bacteria in vegetable soils. Appl Microbiol Biotechnol 99, 5709-5718.

Subramanian, S., Huq, S., Yatsunenko, T., Haque, R., Mahfuz, M., Alam, M.A., Benezra, A., DeStefano, J., Meier, M.F., Muegge, B.D., Barratt, M.J., VanArendonk, L.G., Zhang, Q., Province, M.A., Petri, W.A., Jr., Ahmed, T., Gordon, J.I., 2014. Persistent gut microbiota immaturity in malnourished Bangladeshi children. Nature 510, 417-421.

Tang, Y.-Q., Ji, P., Lai, G.-L., Chi, C.-Q., Liu, Z.-S., Wu, X.-L., 2012. Diverse microbial community from the coalbeds of the Ordos Basin, China. International Journal of Coal Geology 90-91, 21-33.

Tian, H., Lu, C., Ciais, P., Michalak, A.M., Canadell, J.G., Saikawa, E., Huntzinger, D.N., Gurney, K.R., Sitch, S., Zhang, B., Yang, J., Bousquet, P., Bruhwiler, L., Chen, G., Dlugokencky, E., Friedlingstein, P., Melillo, J., Pan, S., Poulter, B., Prinn, R., Saunois, M., Schwalm, C.R., Wofsy, S.C., 2016. The terrestrial biosphere as a net source of greenhouse gases to the atmosphere. Nature 531, 225-228.

Treude, T., Krause, S., Maltby, J., Dale, A.W., Coffin, R., Hamdan, L.J., 2014. Sulfate reduction and methane oxidation activity below the sulfate-methane transition zone in Alaskan Beaufort Sea continental margin sediments: Implications for deep sulfur cycling. Geochimica et Cosmochimica Acta 144, 217-237.

Wang, B., Sun, F., Tang, D., Zhao, Y., Song, Z., Tao, Y., 2015. Hydrological control rule on coalbed methane enrichment and high yield in FZ Block of Qinshui Basin. Fuel 140, 568-577.

Wang, D.T., Welander, P.V., Ono, S., 2016. Fractionation of the methane isotopologues 13CH4, 12CH3D, and 13CH3D during aerobic oxidation of methane by Methylococcus capsulatus (Bath). Geochimica et Cosmochimica Acta 192, 186-202.

Wang, Q., Guo, H., Wang, H., Urynowicz, M.A., Hu, A., Yu, C.-P., Fallgren, P., Jin, S., Zheng, H., Zeng, R.J., Liu, F., Chen, B., Zhang, R., Huang, Z., 2019. Enhanced production of secondary biogenic coalbed natural gas from a subbituminous coal treated by hydrogen peroxide and its geochemical and microbiological analyses. Fuel 236, 1345-1355.

Wei, M., Yu, Z., Jiang, Z., Zhang, H., 2014. Microbial diversity and biogenic methane potential of a thermogenic-gas coal mine. International Journal of Coal Geology 134-135, 96-107.

Wenk, C.B., Zopfi, J., Blees, J., Veronesi, M., Niemann, H., Lehmann, M.F., 2014. Community N and O isotope fractionation by sulfide-dependent denitrification and anammox in a stratified lacustrine water column. Geochimica et Cosmochimica Acta 125, 551-563.

Wong, H.L., White, R.A., 3rd, Visscher, P.T., Charlesworth, J.C., Vazquez-Campos, X., Burns, B.P., 2018. Disentangling the drivers of functional complexity at the metagenomic level in Shark Bay microbial mat microbiomes. ISME J 12, 2619-2639.

Xu, H., Tang, D., Tang, S., Zhang, W., Meng, Y., Gao, L., Xie, S., Zhao, J., 2015. Geologic and hydrological controls on coal reservoir water production in marine coal-bearing strata: A case study of the Carboniferous Taiyuan Formation in the Liulin area, eastern Ordos Basin, China. Marine and Petroleum Geology 59, 517-526.

Yao, Y., Liu, D., Yan, T., 2014. Geological and hydrogeological controls on the accumulation of coalbed methane in the Weibei field, southeastern Ordos Basin. International Journal of Coal Geology 121, 148-159.

Yatsunenko, T., Rey, F.E., Manary, M.J., Trehan, I., Dominguez-Bello, M.G., Contreras, M., Magris, M., Hidalgo, G., Baldassano, R.N., Anokhin, A.P., Heath, A.C., Warner, B., Reeder, J., Kuczynski, J., Caporaso, J.G., Lozupone, C.A., Lauber, C., Clemente, J.C., Knights, D., Knight, R., Gordon, J.I., 2012. Human gut microbiome viewed across age and geography. Nature 486, 222-227.

Zerkle, A.L., Kamyshny, A., Kump, L.R., Farquhar, J., Oduro, H., Arthur, M.A., 2010. Sulfur cycling in a stratified euxinic lake with moderately high sulfate: Constraints from quadruple S isotopes. Geochimica et Cosmochimica Acta 74, 4953-4970.

Zhang, J., Liang, Y., Yau, P.M., Pandey, R., Harpalani, S., 2015. A metaproteomic approach for identifying proteins in anaerobic bioreactors converting coal to methane. International Journal of Coal Geology 146, 91-103.

Zhang, S., Tang, S., Li, Z., Guo, Q., Pan, Z., 2015. Stable isotope characteristics of CBM co-produced water and implications for CBM development: The example of the Shizhuangnan block in the southern Qinshui Basin, China. Journal of Natural Gas Science and Engineering 27, 1400-1411.

Zhang, S., Tang, S., Li, Z., Pan, Z., Shi, W., 2016. Study of hydrochemical characteristics of CBM co-produced water of the Shizhuangnan Block in the southern Qinshui Basin, China, on its implication of CBM development. International Journal of Coal Geology 159, 169-182.

Zopfi, J., Böttcher, M.E., Jørgensen, B.B., 2008. Biogeochemistry of sulfur and iron in Thioploca-colonized surface sediments in the upwelling area off central chile. Geochimica et Cosmochimica Acta 72, 827-843.

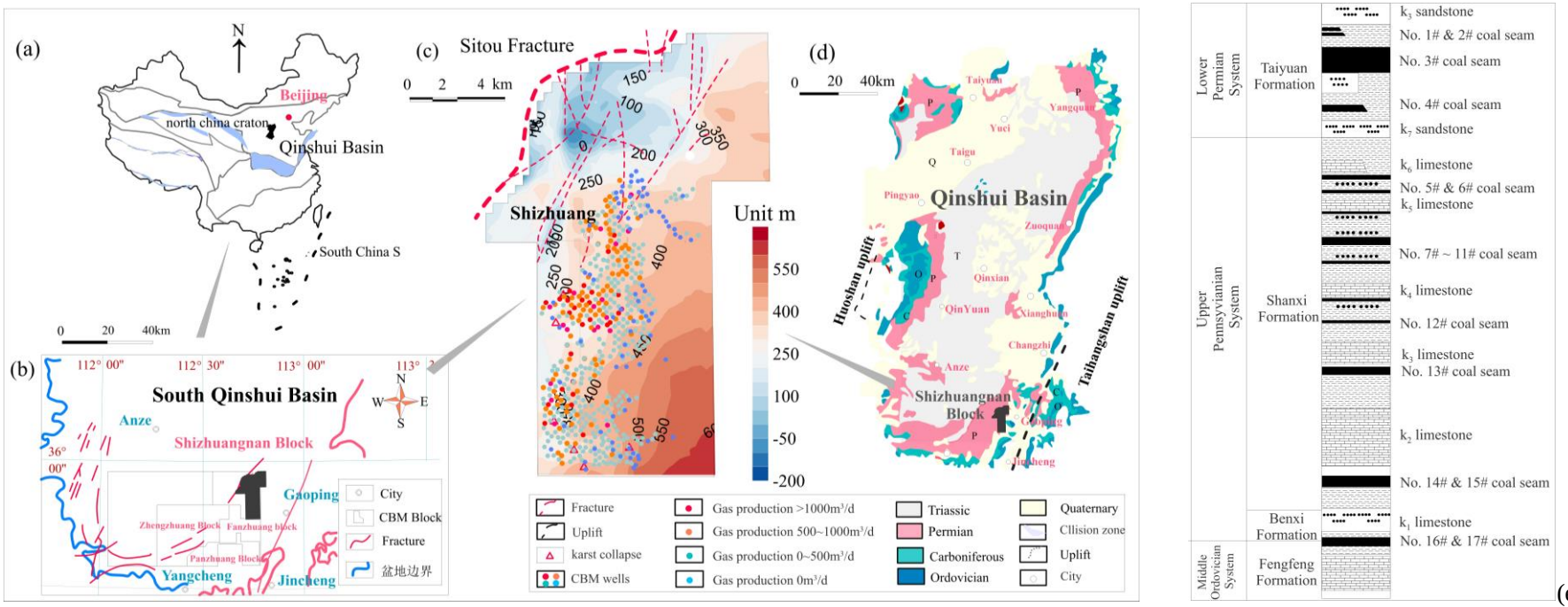

Fig 1. Location of the study area. (a) Location of Qinshui Basin in China; (b) Location of Shizhuangnan Block in Qinshui Basin; (c) Distribution of drainage wells in Shizhuangnan Block, the base map is the elevation contour of 3 # coal seam (m), different drainage well colors represent different daily average gas production, as shown in the legend; (d) Geological map of exposed strata and location of Shizhuangnan Block in Qinshui Basin; (e)Stratigraphic column of the study area.

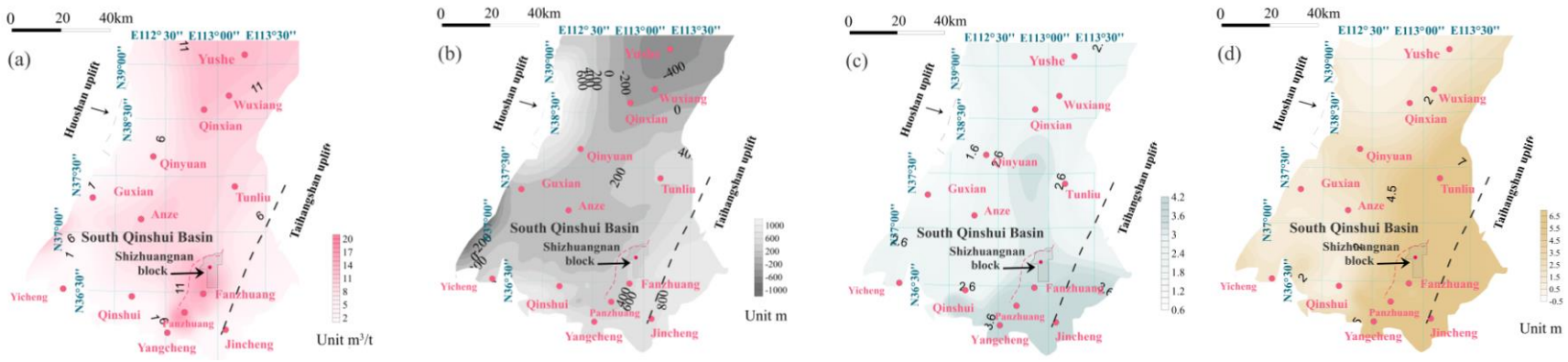

Fig 2. Contour map of 3# coal reservoir characteristics and location of Shizhuangnan Block in Qinshui Basin (a) Contour map of 3# Coal Reservoir's gas content (m^3/t); (b) Contour map of 3# Coal Reservoir's elevation (m); (c) Contour map of 3# Coal Reservoir's vitrinite reflectance; (d)Contour map of 3# Coal Reservoir's thickness (m).

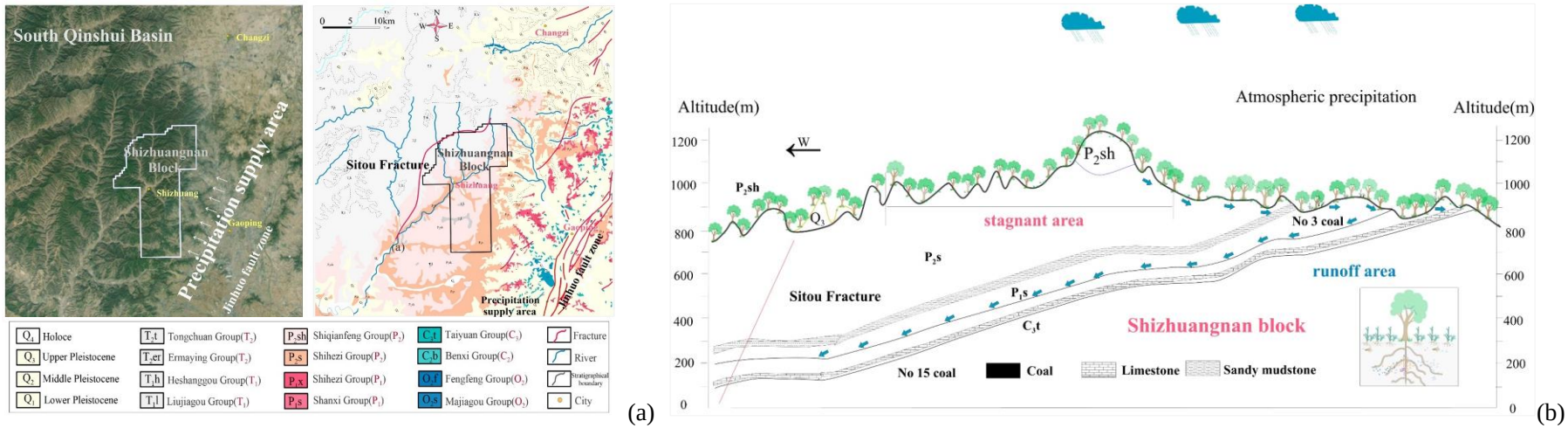

Fig 3. (a) Satellite topographic map and geological map of exposed strata in Shizhuangnan block (b) Sketch map of atmospheric precipitation runoff in study area

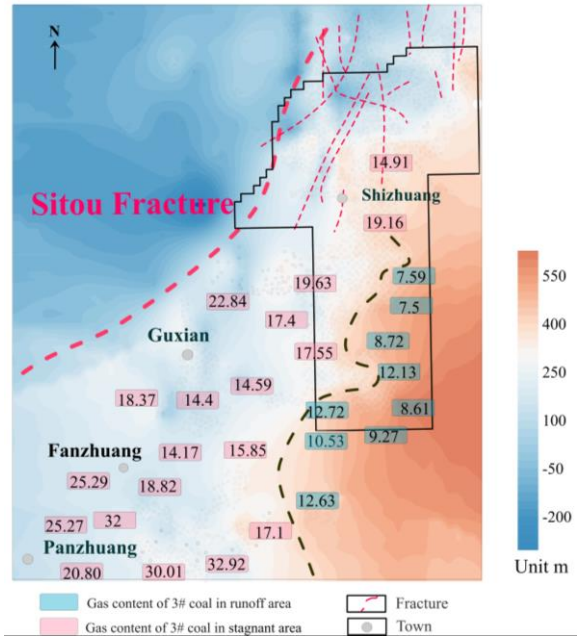

Fig 4. 3# Coal Reservoir's gas content (m^3/t) in Shizhuangnan block, The base map is Contour map of 3# Coal Reservoir's elevation(m), the red dotted line represents Sitou Fracture and the black dotted line represents the boundary line of runoff area and stagnant area

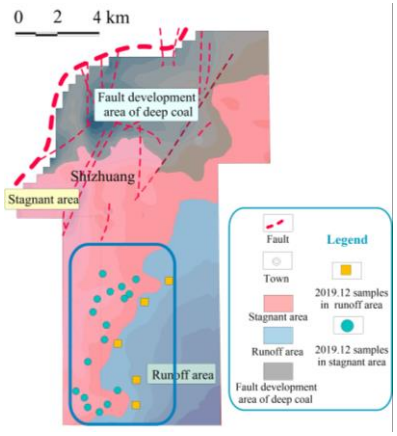

(a)

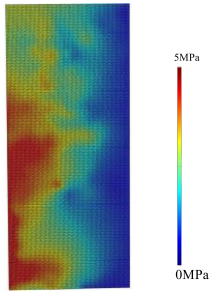

(b)

Fig 5. (a)Sample distribution in study area and division of runoff area and stagnant area (b) Numerical modeling of water pressure (Mpa) in sampling area (Fig.4a within the blue box) by Comsol 5.4.

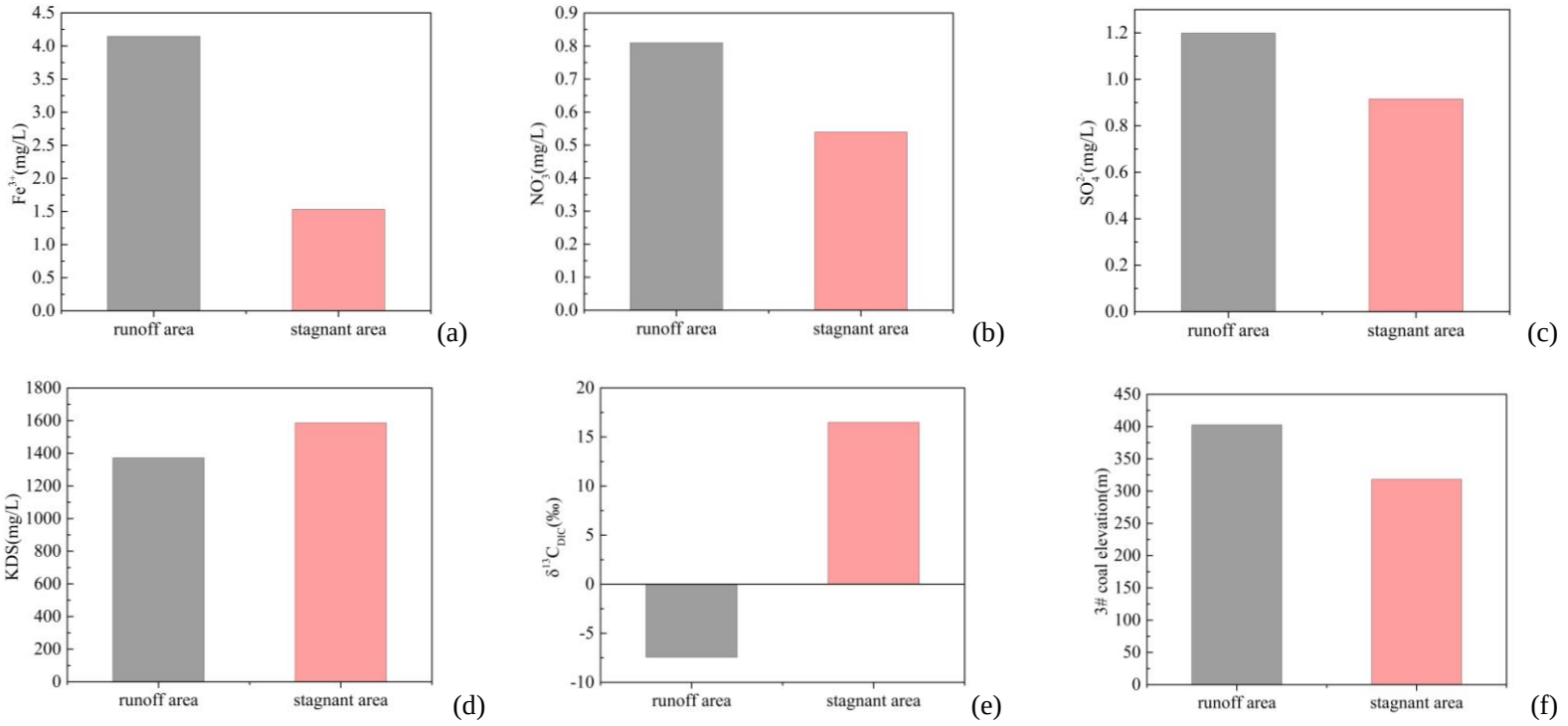

Fig 6. Geochemical characteristics of water ions and gas composition in runoff area and stagnant area (a) Fe^{3+} (mg/L); (b) NO_3^- (mg/L); (c) SO_4^{2-}(mg/L); (d) KDS (mg/L); (e) $\delta^{13}C_{DIC}$(‰); (f) 3# coal elevation(m)

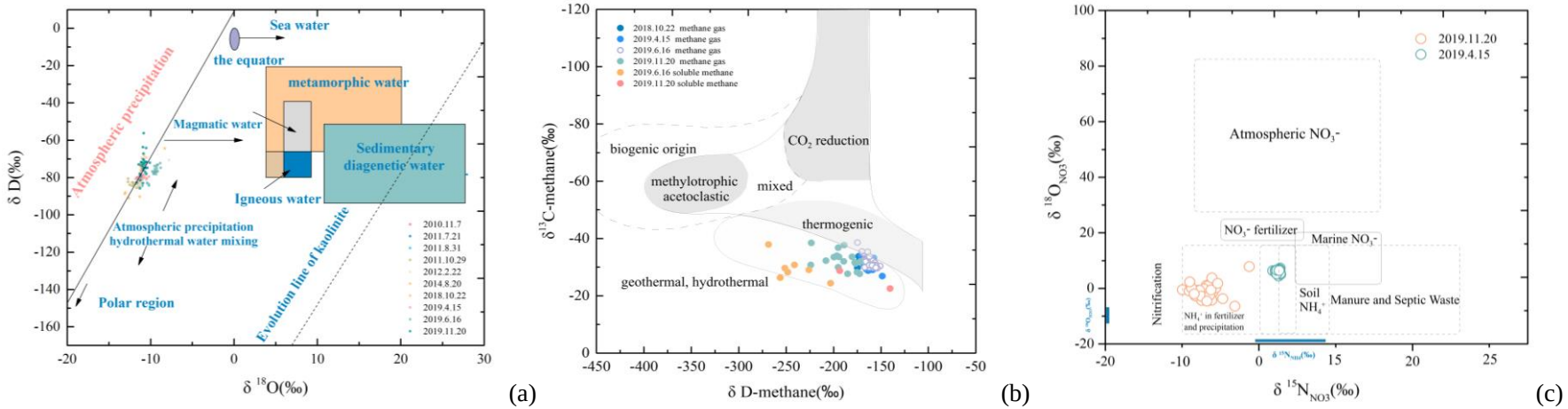

(a) (b) (c)

Fig 7. Isotopic characteristics of water samples in the study area (a) Hydrogen and oxygen isotopes of H_2O(‰) (b) Hydrogen and carbon isotopics of CH_4 (‰) (c) Nitrogen and oxygen isotopic of nitrate (‰). Isotopes data contains our previors samples collected from 2010 to 2019.

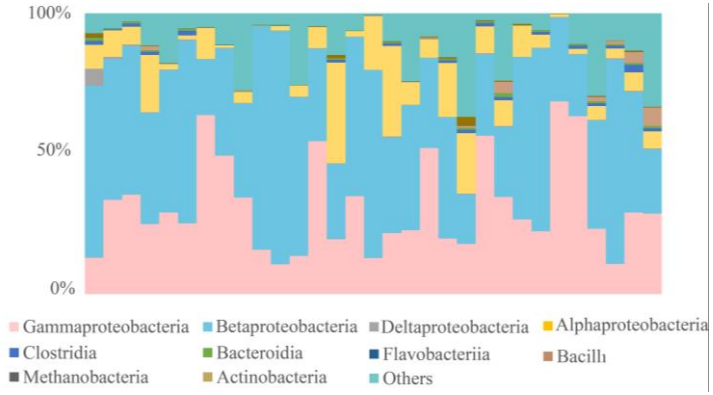

Fig 8(a). Species distribution map of the study area

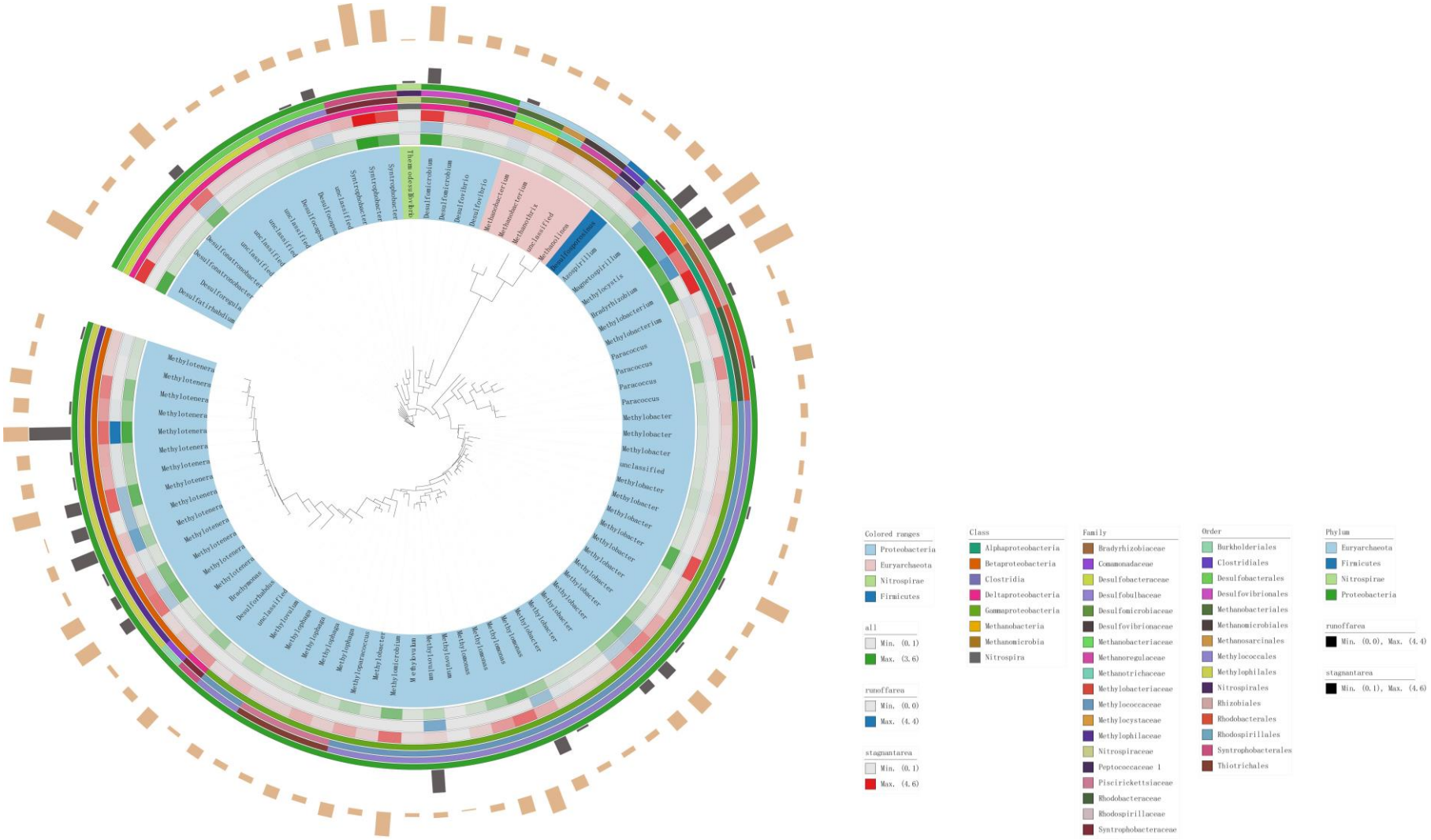

Fig 8(b). Maximum likelihood phylogenetic constructed by using top 90 highly abundant C-N-S microorganisms based on 16s sequences. The outer histogram represents the abundance of selected C-N-S microorganisms. The yellow and black column represent mean abundance of samples in two groups (runoff area, stagnant area). The color of the middle ring represents each microorganism's Class, Family, Order and Phylum.

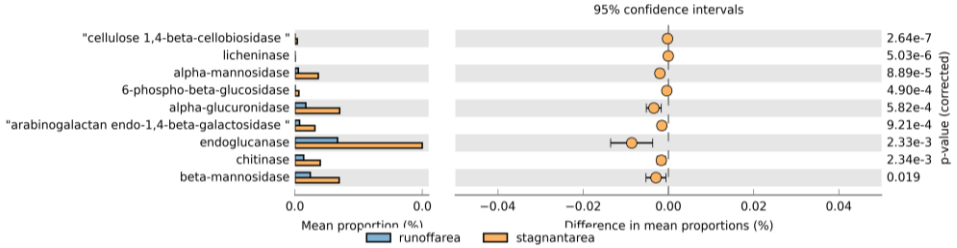

(a)

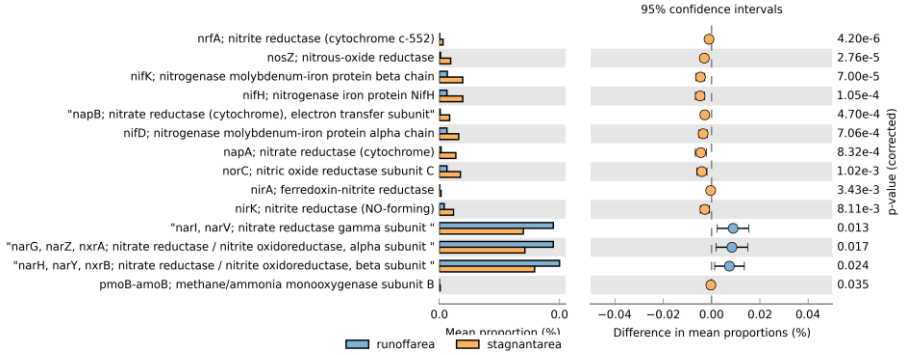

(b)

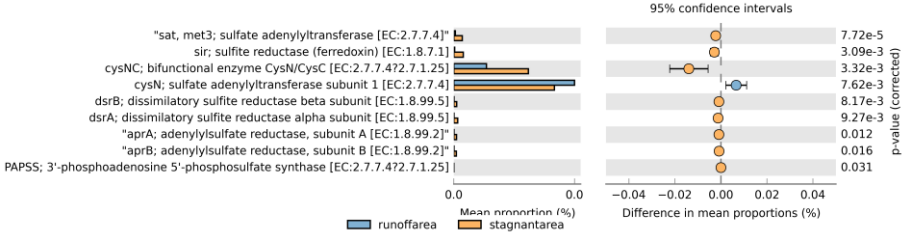

(c)

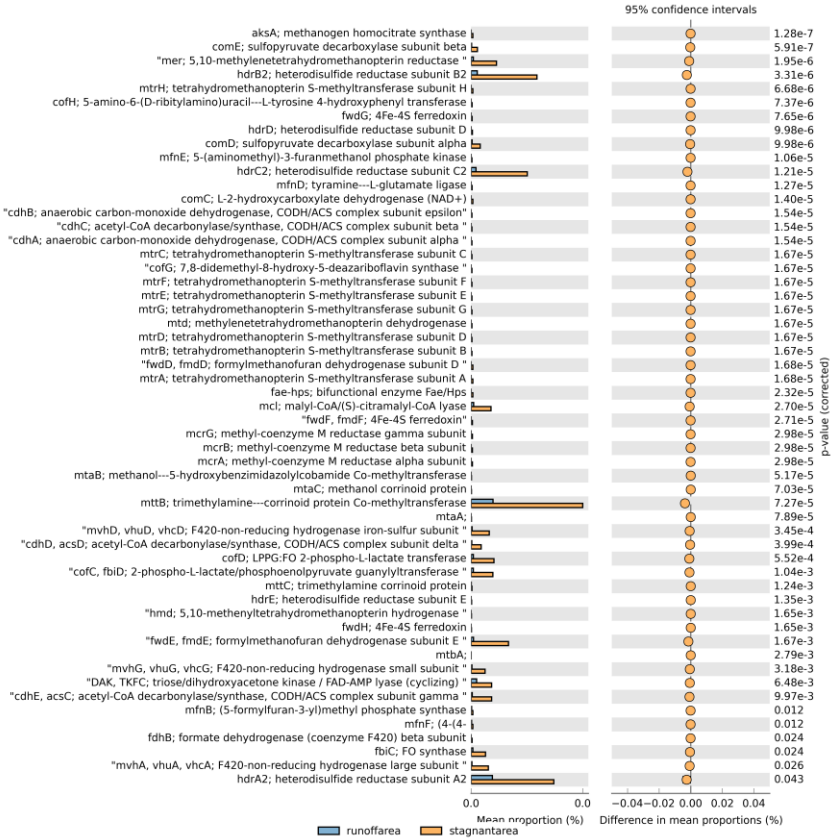

(d)

Fig 9 Analysis of differnet relative abundance of functional genes between runoff area and stagnant area using Welch's t-test with FDR correction in STAMP (95% confidence intevals, q<0.05), the blue color represents runoff area samples, the yellow color represents stagnant area samples. (a) Recalcitrant C decomposition genes; (b) N cycling genes; (c) S cycling genes; (c) Methane metabolism genes

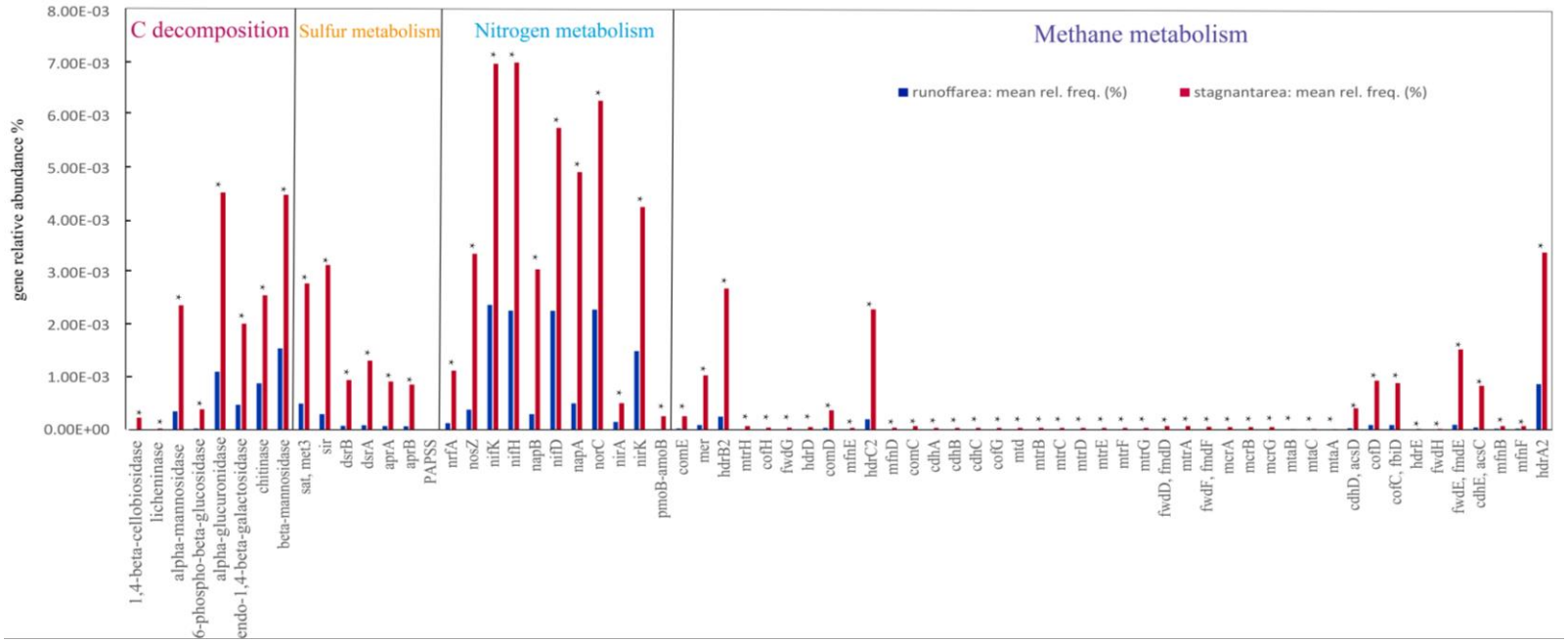

Fig 10 Comparition of differnet functional genes' relative abundence, including C decompositon, Sulfur metabolism, Nitrogen metabolism and Methane metabolism genes between runoff area and stagnant area using Welch's t-test, the dark blue histogram represents runoff area and the red histogram represents stagnant area, * means the gene's difference is significant ($p<0.05$).

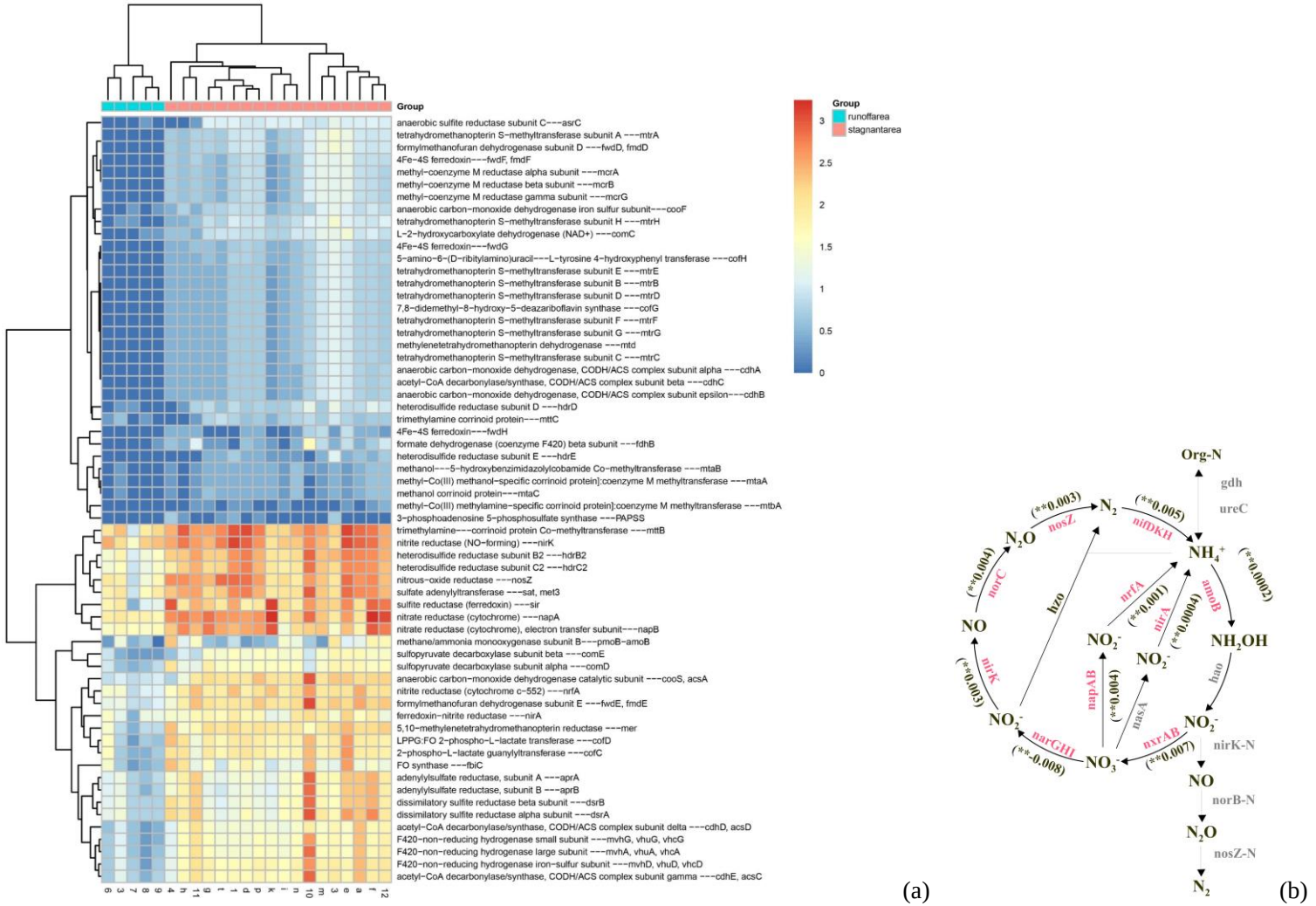

Fig 11 (a) Heatmap shown functional genes' relative abundance of each sample in runoff area and stagnant area. The relative abundance of genes was converted into $\log_{10}$ (relative abundence*10^6) scale for better exhibition in heatmap. (b) N processes from Picrust2 data. The percentage change in N cycling genes' relative abundance in runoff area and stagnant area was indicated in parenthesis, ** means the gene's difference is significant ($p<0.05$). Genes whose change in relative abundance is significant ($p<0.05$) were labelled in red. Grey-coloured genes were not targeted by the Picrust2 data used here, not detected or not applicable.

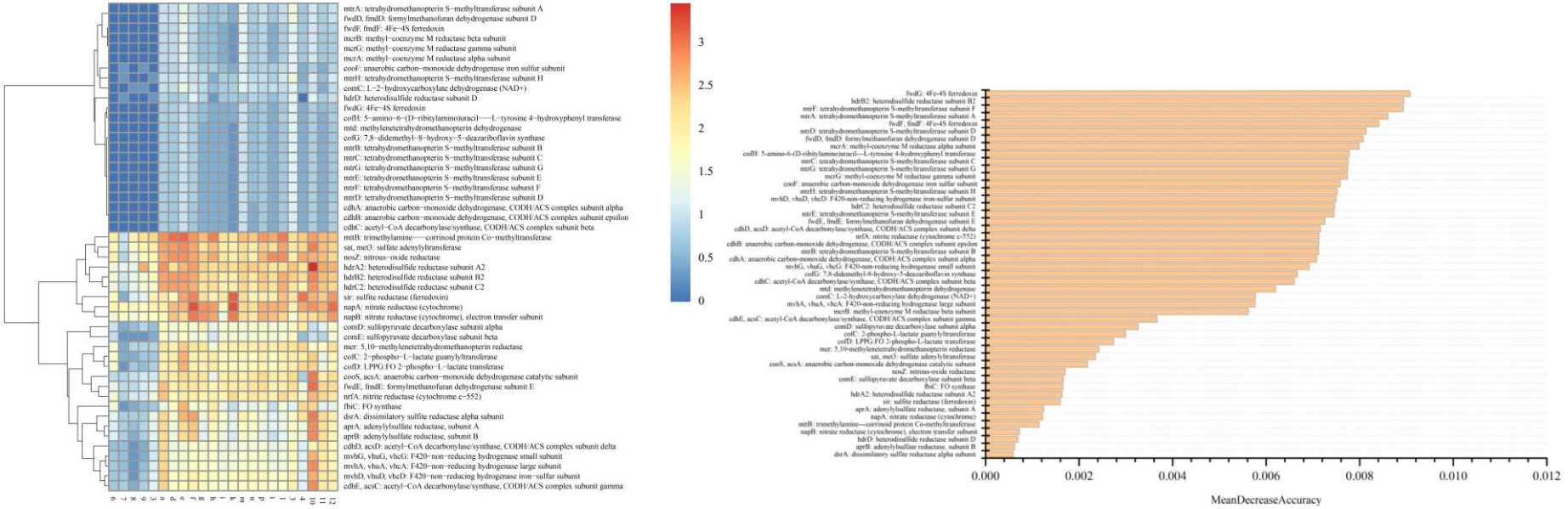

Fig 12 (a) Heatmap shown functional genes' relative abundence that changes significantly between runoff area and stagnant area, these genes were choosen by the machine learning caculation. The genes' relative abundence was converted to $\log_{10}$ (relative abundence*10^6) for better exhibition in heatmap. (b) The importance ranking of MeanDreaseAccuracy caculated by randomforest packages.

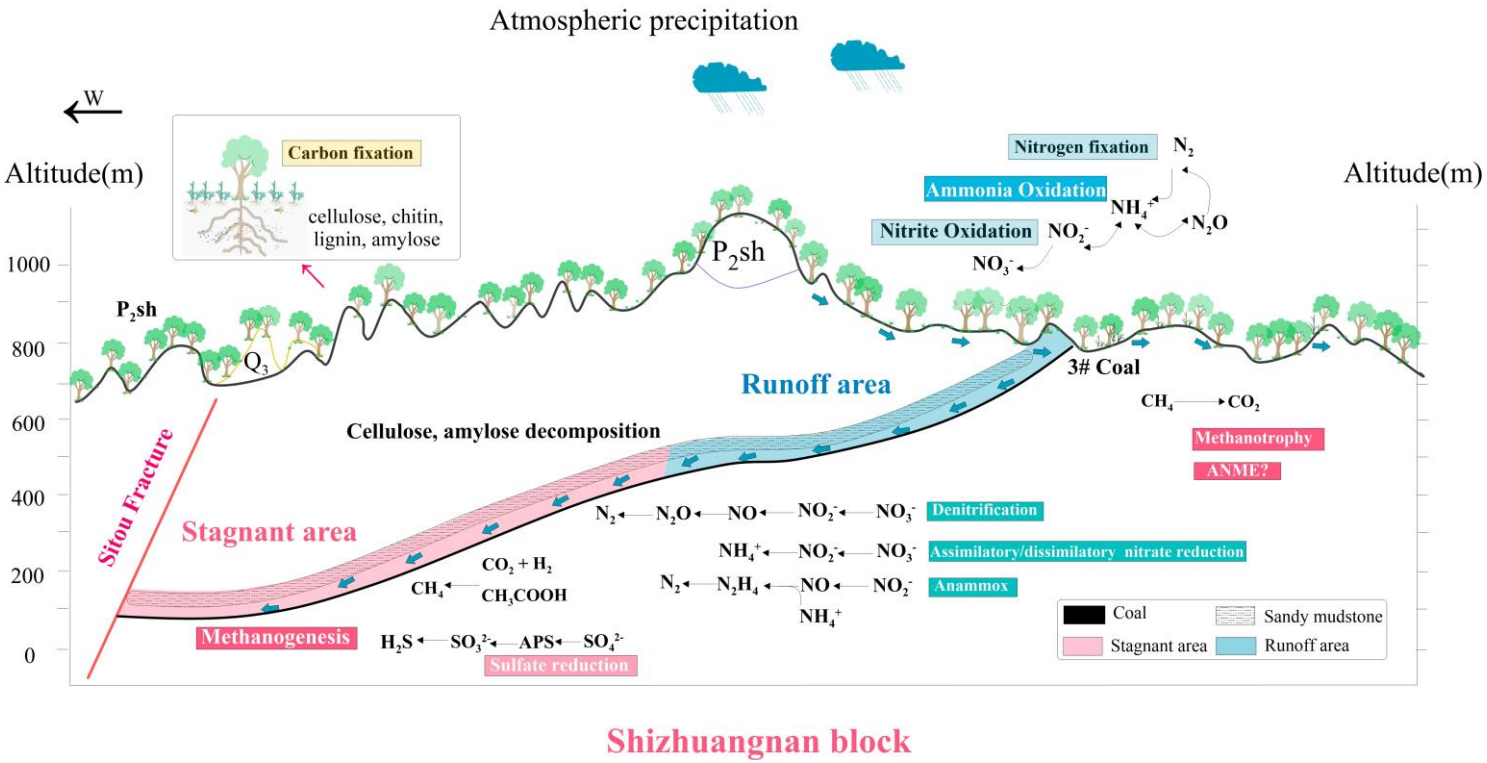

Fig 13 Microbial C-N-S cycle pattern in Shizhuangnan Block

Table 1 Significance tests on the effects of hydrodynamic conditions on the microbial community functional structure

	MRPP		Adonis		ANOSIM	
Bray	δ	p	F	p	R	p
	0.7104	0.004	4.6536	0.003	0.5192	0.001

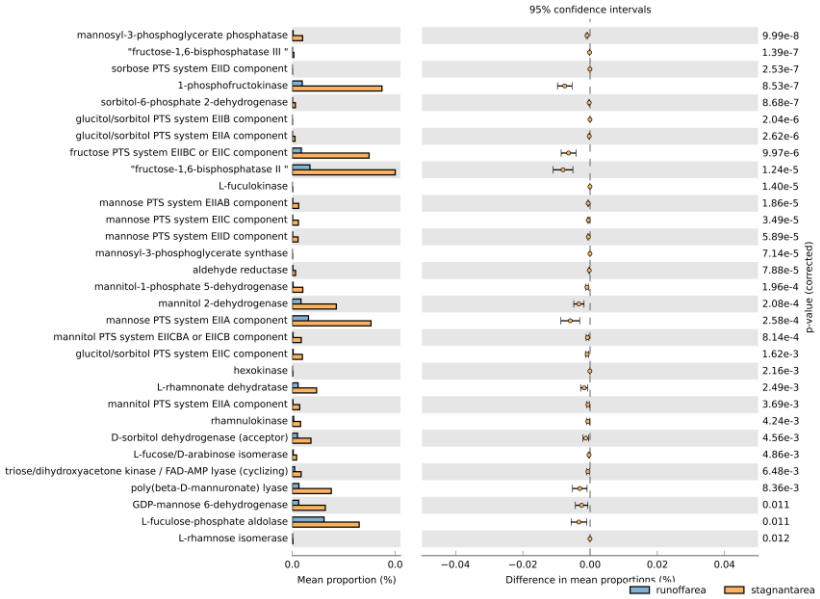

(a)Fructose and mannose metabolism

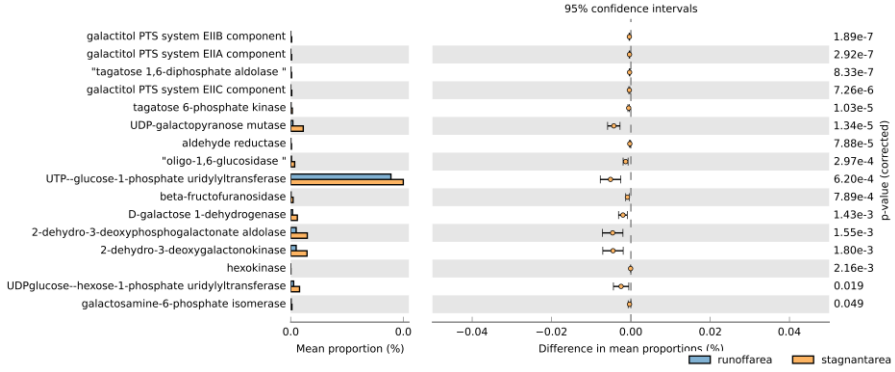

(b)Galactose metabolism

Supplementary Fig 1 Analysis of differnet functional genes of C-N-S microorganism between runoff area and stagnant area using Welch's t-test with FDR correction in STAMP (95% confidence intevals, q<0.05) (a) Fructose and mannose metabolism; (b) Galactose metabolism. The blue color represents runoff area samples, the yellow color represents stagnant area samples.